

Trinucleon Photo Reactions with Δ -Isobar Excitation: Radiative Nucleon-Deuteron Capture and Two-Body Photo Disintegration of the Three-Nucleon Bound State

L. P. Yuan¹, K. Chmielewski¹, M. Oelsner¹, P. U. Sauer¹, A. C. Fonseca², and
J. Adam Jr.³

¹ Institut für Theoretische Physik, Universität Hannover, Appelstraße 2,
D-30167 Hannover, Germany

² Centro Física Nuclear da Universidade de Lisboa, Av. Prof. Gama Pinto,
Nº2, P-1649-003 Lisboa, Portugal

³ Nuclear Physics Institute, Academy of Sciences of Czech Republic, CZ-
25068, Řež, Czech Republic

Abstract. Radiative nucleon-deuteron capture and photo disintegration of the three-nucleon bound state with two-body final states are described. The description uses nucleon degrees of freedom extended to include the excitation of a single nucleon to a Δ -isobar. The baryonic interaction and the electromagnetic current couple nucleonic states and states with a Δ -isobar. Exact solutions of three-particle scattering equations are employed for the initial or final states of the reactions. The current has one-baryon and two-baryon contributions. The role of the Δ -isobar in the description of the considered photo reactions is discussed and found to be moderate. The spin observables A_{yy} and T_{20} at 90° lab scattering angle can be calculated model-independently from the $E1$ Siegert term in the long-wavelength limit.

1 Introduction

Trinucleon photo reactions are theoretically described. Only reactions with two-body initial or final states are discussed, not three-body photo disintegration of the three-nucleon bound state. The considered reaction energies are well above three-nucleon break-up, but remain otherwise low, i.e., below 50 MeV in the three-nucleon c.m. system.

The present calculation of trinucleon photo reactions extends the description of elastic and inelastic nucleon-deuteron scattering given by some of the authors in refs. [1–4]. Nucleon-deuteron scattering is studied in general [5], in order to search for unambiguous signals of a three-nucleon force. Indeed, discrepancies between theoretical predictions, derived from two-nucleon potentials, and experimental data got uncovered [3, 6]. In the same spirit trinucleon photo reactions are studied, in order to find clear indications for the working of a three-nucleon force and of corresponding two- and three-nucleon electromagnetic (e.m.) exchange currents.

The theoretical description of trinucleon photo reactions, given in this paper, is realistic in the following sense: A realistic nuclear interaction is employed when solving for the hadronic states involved, i.e., for the trinucleon bound state and for the nucleon-deuteron scattering states. The employed nuclear interaction is a hermitian coupled-channel two-baryon potential between nucleons which allows for the excitation of a single nucleon to a Δ -isobar. The Δ -isobar mediates an effective three-nucleon force. However, the Coulomb interaction between the two protons is not taken into account. Thus, the calculations of this paper are done for photo reactions on ${}^3\text{H}$, though most experimental data will refer to photo reactions on ${}^3\text{He}$. The nuclear current is built-up from one-baryon and two-baryon contributions. The current contributions contain, for reasons of consistency, pieces with transitions to one-baryon and two-baryon states with a single Δ -isobar. The description of the considered reactions is comparatively transparent: As long as only a few multipoles of the current determine the observables, only few total angular momenta are picked out from the nucleon-deuteron scattering states.

The calculation of trinucleon elastic and inelastic nucleon-deuteron scattering, given in refs. [1–4], is based on a separable expansion of the two-baryon transition matrix; the same separable expansion is used here for the description of photo reactions. In the separable treatment of the hadronic interaction, our calculation corresponds to the work of refs. [7, 8]; however, it is more complete with respect to the employed current. Our calculation attempts to be as realistic as the description given in refs. [9, 10], which does not require a separable expansion of the hadronic interaction. In contrast, the addition of the Δ -isobar degree of freedom gives our calculation a new theoretical dimension. The calculation will attempt to isolate the effects arising from the Δ -isobar. Preliminary results were presented in ref. [11].

Sect. 2 describes the calculational apparatus. Sect. 3 shows and discusses results. Sect. 4 is a summary with conclusions.

2 Calculation Procedure

2.1 Basic Elements of Calculation

The basic building block for the description of photo reactions is the e.m. hamiltonian

$$H_I^{e.m.} = \frac{1}{c} \int d^3x J^\mu(x) A_\mu(x)|_{x_0=0}, \quad (2.1)$$

which couples baryonic states to the photon (γ). The operators in Eq. (2.1) depend on space-time x , but are to be used as Schrödinger operators at time $x_0 = 0$; $A_\mu(x)$ is the photon field operator, which we parametrize in the form

$$A_\mu(x) = \frac{(4\pi)^{1/2} \hbar c}{(2\pi)^{3/2}} \int \frac{d^3k_\gamma}{\sqrt{2k_{\gamma 0} c}} \sum_{\lambda=0}^3 [a_\lambda(\mathbf{k}_\gamma) \epsilon_\mu(\mathbf{k}_\gamma, \lambda) e^{-\frac{i}{\hbar} k_\gamma x} + a_\lambda^\dagger(\mathbf{k}_\gamma) \epsilon_\mu^*(\mathbf{k}_\gamma, \lambda) e^{\frac{i}{\hbar} k_\gamma x}] |_{k_{\gamma 0}=|\mathbf{k}_\gamma|}. \quad (2.2)$$

The polarizations $\lambda = 1, 2$ correspond to those of a real transverse photon; $\epsilon_\mu(\mathbf{k}_\gamma, \lambda)$ are the polarization vectors, constrained by $k_\gamma^\mu \epsilon_\mu(\mathbf{k}_\gamma, \lambda) = 0$. A single-photon state of definite momentum \mathbf{k}_γ and polarization λ , δ -function normalized, is $|\mathbf{k}_\gamma, \lambda\rangle = a_\lambda^\dagger(\mathbf{k}_\gamma)|0\rangle$.

The e.m. current operator $J^\mu(x)$ acts in the baryonic Hilbert space which we take to have two sectors, i.e., a purely nucleonic one and one in which one nucleon (N) is turned into a Δ -isobar. The two Hilbert sectors are displayed in Fig. 1 for a three-baryon system as ${}^3\text{He}$. We use the current operator in its Fourier-transformed form, i.e.,

$$J^\mu(\mathbf{Q}) = \int d^3x e^{\frac{i}{\hbar} \mathbf{Q} \cdot \mathbf{x}} J^\mu(x)|_{x_0=0}, \quad (2.3)$$

and employ — specializing to a three-baryon system — a momentum-space representation, based on the Jacobi momenta ($\mathbf{p}\mathbf{q}\mathbf{K}$) of three particles in the definition of ref. [1], i.e.,

$$\langle \mathbf{K}' \mathbf{p}' \mathbf{q}' | J^\mu(\mathbf{Q}) | \mathbf{K} \mathbf{p} \mathbf{q} \rangle = \delta(\mathbf{K}' - \mathbf{Q} - \mathbf{K}) \langle \mathbf{p}' \mathbf{q}' | j^\mu(\mathbf{Q}, \mathbf{K}' + \mathbf{K}) | \mathbf{p} \mathbf{q} \rangle. \quad (2.4)$$

In Eq. (2.4) \mathbf{Q} is the three-momentum transfer by the photon; it will take on particular values depending on the considered reaction; in e.m. reactions with real photons it is given by the photon momentum \mathbf{k}_γ . A total-momentum conserving δ -function is split off; the remaining current operator $j^\mu(\mathbf{Q}, \mathbf{K}' + \mathbf{K})$ only acts on the internal momenta of the three-baryon system with a parametric dependence on the combination $\mathbf{K}' + \mathbf{K}$ of total momenta. Since all meson degrees of freedom are frozen, the operator has one-baryon and many-baryon pieces. Besides the standard nucleonic-current part there are additional parts involving the Δ -isobar. We take one-baryon and two-baryon contributions into account, shown in Figs. 2 - 4. The horizontal lines in the diagrams indicate that the meson exchanges are instantaneous. The exchanged mesons are the

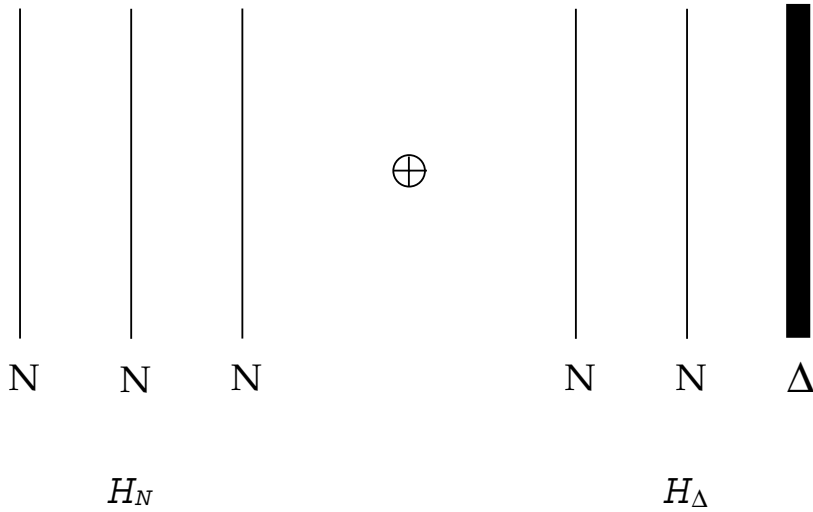


Figure 1. Hilbert space considered. It consists of a purely nucleonic sector \mathcal{H}_N and a sector \mathcal{H}_Δ in which one nucleon is turned into a Δ -isobar, indicated by a thick vertical line.

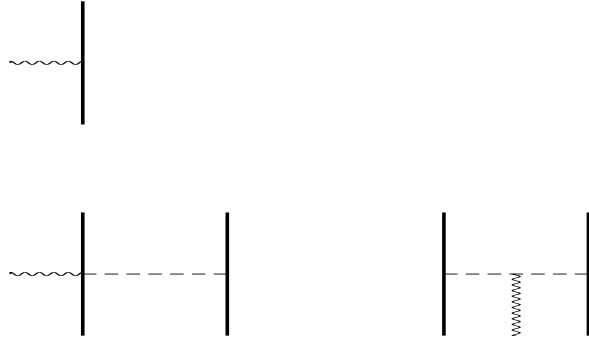


Figure 2. One- and two-baryon processes contained in the used e.m. current. The dashed horizontal line indicates instantaneous meson exchange. Diagonal π - and ρ -exchanges are taken into account as well as the nondiagonal $\rho\pi\gamma$ and $\omega\pi\gamma$ contributions. In this figure only purely nucleonic processes are depicted.

pion (π) and the rho (ρ). The nondiagonal $\rho\pi\gamma$ and $\omega\pi\gamma$ contributions, ω denoting the isoscalar vector meson omega, are also taken into account for the purely nucleonic current of Fig. 2. The current of Fig. 3 couples purely nucleonic states with states containing one Δ -isobar; the hermitian adjoint pieces are not diagrammatically shown; the nondiagonal $\rho\pi\gamma$ and $\omega\pi\gamma$ contributions

to the two-baryon current involving one Δ -isobar are not considered. Among the contributions between Δ -isobar states only the one of one-baryon nature is kept as shown in Fig. 4. The current is derived by the extended S -matrix method of refs. [12–15]; it satisfies current conservation with the corresponding π - and ρ -exchanges in the coupled-channel two-baryon interaction H_I of one-boson exchange nature. The current is systematically expanded up to first order in p/m_N , \mathbf{p} being a characteristic baryon momentum and m_N the nucleonic rest mass.

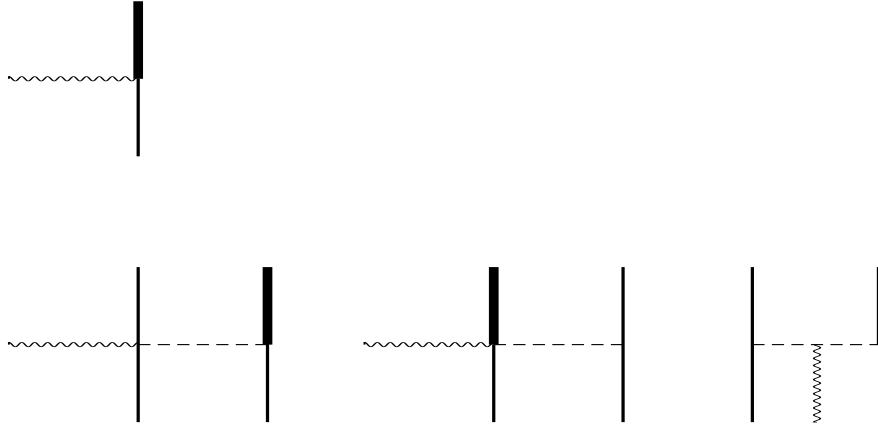


Figure 3. One- and two-baryon processes contained in the used e.m. current. In this figure processes are depicted in which one nucleon is turned into a Δ -isobar. The hermitian adjoint processes are taken into account, but are not diagrammatically shown.

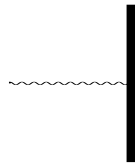


Figure 4. One-baryon process contained in the used e.m. current. It is the only process between Δ -isobar states which is considered.

In the perturbative spirit for the evolution of photo processes, the e.m. interaction $H_I^{e.m.}$ acts only once, whereas the hadronic interaction H_I has exactly to be taken into account up to all orders. We use hadronic channel states, seen in the initial and final states $|i\mathbf{P}_i\rangle$ and $|f\mathbf{P}_f\rangle$ of the photo reactions, in the

form

$$|\Phi_B \mathbf{p}_B\rangle = |B\rangle |\mathbf{p}_B\rangle, \quad (2.5a)$$

$$|\Phi_\alpha(\mathbf{q})\nu_\alpha(Nd)\mathbf{K}\rangle = |\phi_\alpha(\mathbf{q})\nu_\alpha(Nd)\rangle |\mathbf{K}\rangle, \quad (2.5b)$$

with the energies

$$E_B(\mathbf{p}_B) = m_B c^2 + \frac{\mathbf{p}_B^2}{6m_N}, \quad (2.6a)$$

$$E_{Nd}(\mathbf{q}\mathbf{K}) = m_N c^2 + m_d c^2 + \frac{\mathbf{q}^2}{4m_N/3} + \frac{\mathbf{K}^2}{6m_N}, \quad (2.6b)$$

m_N, m_d and m_B being the rest masses of nucleon, deuteron and trinucleon bound state. The internal trinucleon bound state is $|B\rangle$, which is normalized to 1. The product nucleon-deuteron channel state in the three-nucleon c.m. frame is $|\phi_\alpha(\mathbf{q})\nu_\alpha(Nd)\rangle$ in the notation of ref. [1], ν_α denoting all discrete quantum numbers. In both cases the c.m. motion is explicitly added to the internal motion; in the three-nucleon channel with a photon, the total momentum \mathbf{P} is different from the total momentum $\mathbf{K} = \mathbf{p}_B$ of the three nucleons, bound in the trinucleon bound state $|B\rangle$.

The matrix elements of the e.m. interaction require fully correlated hadronic states, i.e.,

$$|\Phi_B \mathbf{p}_B\rangle = \pm i0G(E_B(\mathbf{p}_B) \pm i0)|B\rangle |\mathbf{p}_B\rangle, \quad (2.7a)$$

$$|\Psi_\alpha^{(\pm)}(\mathbf{q})\nu_\alpha(Nd)\mathbf{K}\rangle = \pm i0G(E_{Nd}(\mathbf{q}\mathbf{K}) \pm i0)(1+P)/\sqrt{3}|\Phi_\alpha(\mathbf{q})\nu_\alpha(Nd)\mathbf{K}\rangle, \quad (2.7b)$$

with the full resolvent

$$G(Z) = \frac{1}{Z - H_0 - H_I}; \quad (2.8)$$

the free Hamiltonian H_0 contains the motion of the center of mass; P symmetrizes the nucleon-deuteron product state; the individual kinetic energy operators are of nonrelativistic form; they yield the eigenvalues of Eqs. (2.6). The hadronic state (2.7b) is normalized to the delta function without additional normalization factors. Since the hadronic interaction Hamiltonian H_I acts on relative coordinates only, the full resolvent reproduces the bound state $|B\rangle$ and correlates the nucleon-deuteron scattering state only in its internal part, i.e.,

$$|\Psi_\alpha^{(\pm)}(\mathbf{q})\nu_\alpha(Nd)\mathbf{K}\rangle = |\psi_\alpha^{(\pm)}(\mathbf{q})\nu_\alpha(Nd)\rangle |\mathbf{K}\rangle. \quad (2.9)$$

2.2 S -Matrix for Trinucleon Photo Reactions

The kinematics of the considered processes is shown in Fig. 5. The figure also defines the employed notation for the individual particle momenta; p_N, p_d, p_B and k_γ are on-mass-shell four-momenta. The corresponding particle energies

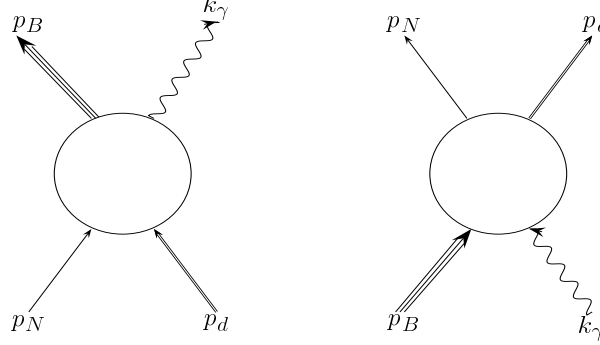


Figure 5. Schematic description of the considered photo reactions of the deuteron. The lines for the two-baryon and three-baryon particles are drawn in a special form to indicate their compositeness.

are derived from the zero components of those momenta, i.e., $E_N(\mathbf{p}_N) = p_{N0}c$, $E_d(\mathbf{p}_d) = p_{d0}c$ and $E_B(\mathbf{p}_B) = p_{B0}c$; they are relativistic ones in contrast to those of the nonrelativistic model calculation in Eqs. (2.6) for which the same symbols are used; we shall make sure in the following that no confusion arises.

The S -matrix and the differential cross sections take the forms given in the following subsections.

2.2.1 Radiative Capture in Nucleon-Deuteron Scattering

We give various alternative forms for the S -matrix elements:

$$\begin{aligned} \langle f\mathbf{P}_f|S^{rc}|i\mathbf{P}_i\rangle &= (-i)(2\pi\hbar)^4\delta(k_\gamma + p_B - p_N - p_d)\langle s_f|M^{rc}|s_i\rangle \\ &\times \frac{1}{(2\pi\hbar)^6} \frac{1}{\sqrt{2k_{\gamma 0}c} 2E_B(\mathbf{p}_B)2E_N(\mathbf{p}_N)2E_d(\mathbf{p}_d)}, \end{aligned} \quad (2.10a)$$

$$\begin{aligned} \langle f\mathbf{P}_f|S^{rc}|i\mathbf{P}_i\rangle &= (-2\pi i)\delta(k_{\gamma 0}c + E_B(\mathbf{p}_B) - E_N(\mathbf{p}_N) - E_d(\mathbf{p}_d)) \\ &\times \langle f\mathbf{P}_f|H_I^{e.m.}i0G(E_i + i0)|i\mathbf{P}_i\rangle, \end{aligned} \quad (2.10b)$$

$$\begin{aligned} \langle f\mathbf{P}_f|S^{rc}|i\mathbf{P}_i\rangle &= (-2\pi i)\delta(k_{\gamma 0}c + E_B(\mathbf{p}_B) - E_N(\mathbf{p}_N) - E_d(\mathbf{p}_d)) \\ &\times \delta(\mathbf{k}_\gamma + \mathbf{p}_B - \mathbf{p}_N - \mathbf{p}_d) \frac{1}{c} \frac{\sqrt{4\pi\hbar c}}{\sqrt{2k_{\gamma 0}c}} \frac{1}{(2\pi\hbar)^{3/2}} \epsilon_\mu^*(\mathbf{k}_\gamma, \lambda) \\ &\times \langle B|j^\mu(-\mathbf{k}_\gamma, \mathbf{p}_B + \mathbf{p}_N + \mathbf{p}_d)|\psi_\alpha^{(+)}(\mathbf{q}_i)\nu_{\alpha_i}(Nd)\rangle_{\mathbf{q}_i = \frac{\mathbf{p}_d - 2\mathbf{p}_N}{3}}; \end{aligned} \quad (2.10c)$$

$\langle s_f | M^{rc} | s_i \rangle$ is the singularity-free matrix element for radiative capture, from which the differential cross section

$$d\sigma^{rc} = \left| \langle s_f | M^{rc} | s_i \rangle \right|^2 \frac{dLips(p_N + p_d, k_\gamma, p_B)}{4c^2 \sqrt{(p_N \cdot p_d)^2 - m_N^2 m_d^2 c^4}} \quad (2.11a)$$

is obtained. Its dependence on the spin projections m_{s_i} and M_{I_i} of nucleon and deuteron in the initial channel, collectively described by s_i , and on the helicity λ and on the spin projection \mathcal{M}_{B_f} of photon and trinucleon bound state in the final channel, collectively described by s_f , are explicitly indicated. $\langle s_f | M^{rc} | s_i \rangle$ is Lorentz-invariant and can be calculated in any frame. It is defined by

$$\begin{aligned} \langle s_f | M^{rc} | s_i \rangle &= \frac{\sqrt{4\pi}}{c} (2\pi\hbar)^{3/2} \sqrt{2E_B(\mathbf{p}_B) 2E_N(\mathbf{p}_N) 2E_d(\mathbf{p}_d)} \\ &\times \langle B | j^\mu(-\mathbf{k}_\gamma, \mathbf{p}_B + \mathbf{p}_N + \mathbf{p}_d) \epsilon_\mu^*(\mathbf{k}_\gamma, \lambda) | \psi_\alpha^{(+)}(\mathbf{q}_i) \nu_{\alpha_i}(Nd) \rangle \Big|_{\mathbf{q}_i = \frac{\mathbf{p}_d - 2\mathbf{p}_N}{3}} \end{aligned} \quad (2.11b)$$

according to Eqs. (2.10). It contains our model description of the hadronic and e.m. interactions which will — for example with respect to experimental energies — not be fully precise. The model description uses nonrelativistic energies for all hadrons involved. Since the matrix element in (2.11b) can be calculated in any frame, we choose the c.m. frame, i.e., $\mathbf{p}_d = -\mathbf{p}_N$, $\mathbf{p}_B = -\mathbf{k}_\gamma$, and the following computational strategy:

- The experimental deuteron energy in the lab frame determines the total energy of the system and the relative momentum \mathbf{q}_i in the initial channel. This step is done using relativistic kinematics.
- All hadron energies involved in the matrix element (2.11b) are chosen nonrelativistically and consistent with their model values.
- Taking the computed trinucleon binding energy for calculating the rest mass m_B and the average nucleon mass for the nucleon mass m_N , i.e., $m_N c^2 = 938.919$ MeV, the magnitude of the photon momentum $|\mathbf{k}_\gamma|$ is determined employing the nonrelativistic forms (2.6) for the hadron energies, i.e., $|\mathbf{k}_\gamma c| + m_B c^2 + \mathbf{k}_\gamma^2 / 6m_N = m_N c^2 + m_d c^2 + \mathbf{q}_i^2 / (4m_N/3)$. Since the model rest mass m_B is not the experimental one, neither for ${}^3\text{He}$ nor for ${}^3\text{H}$ reactions, the photon momentum does not have the experimental value.

The other building blocks for the differential cross section (2.11a) are the Lorentz-invariant phase-space element $dLips(p_N + p_d, k_\gamma, p_B)$, i.e.,

$$\begin{aligned} dLips(p_N + p_d, k_\gamma, p_B) &= \\ (2\pi\hbar)^4 \delta(k_\gamma + p_B - p_N - p_d) &\frac{d^3 k_\gamma}{(2\pi\hbar)^3 2k_{\gamma 0} c} \frac{d^3 p_B}{(2\pi\hbar)^3 2E_B(\mathbf{p}_B)}, \end{aligned} \quad (2.12)$$

and the incoming flux $4c^2 \sqrt{(p_N \cdot p_d)^2 - m_N^2 m_d^2 c^4}$. In contrast to the matrix element $\langle s_f | M^{rc} | s_i \rangle$ which contains our model assumptions, the kinematic parts

of the differential cross section, the Lorentz-invariant phase-space element and the incoming flux, have to be calculated with the true experimental and relativistic energies of nucleon, deuteron and trinucleon bound state. In the c.m. system the differential cross section takes the form

$$\left. \frac{d\sigma_{c.m.}^{rc}}{d^2\hat{\mathbf{k}}_\gamma} \right|_{s_i \rightarrow s_f} = \frac{1}{64\pi^2} \frac{1}{(\hbar c)^2} \left| \langle s_f | M^{rc} | s_i \rangle \right|^2 \frac{|\mathbf{k}_\gamma|}{|\mathbf{p}_N| (E_N(\mathbf{p}_N) + E_d(\mathbf{p}_N))^2}. \quad (2.13a)$$

That form of the cross section still describes the transition between specified spin states. The spin-averaged differential cross section is

$$\overline{\left. \frac{d\sigma_{c.m.}^{rc}}{d^2\hat{\mathbf{k}}_\gamma} \right|_{s_i \rightarrow s_f}} = \frac{1}{6} \sum_{M_{N_i} M_{d_i}} \sum_{\lambda M_{B_f}} \left. \frac{d\sigma_{c.m.}^{rc}}{d^2\hat{\mathbf{k}}_\gamma} \right|_{s_i \rightarrow s_f}. \quad (2.13b)$$

2.2.2 Two-Body Photo Disintegration of the Trinucleon Bound State

The definitions of the S -matrix $\langle f \mathbf{P}_f | S^{dis} | i \mathbf{P}_i \rangle$, of the singularity-free matrix element $\langle s_f | M^{dis} | s_i \rangle$ and of the differential cross section are similar to those of radiative capture in Eqs. (2.10)–(2.13). However, the initial and final states are interchanged and $\epsilon_\mu^*(\mathbf{k}_\gamma, \lambda)$ is replaced by $\epsilon_\mu(\mathbf{k}_\gamma, \lambda)$. The singularity-free matrix element is defined by

$$\begin{aligned} \langle s_f | M^{dis} | s_i \rangle &= \frac{\sqrt{4\pi}}{c} (2\pi\hbar)^{3/2} \sqrt{2E_B(\mathbf{p}_B) 2E_N(\mathbf{p}_N) 2E_d(\mathbf{p}_d)} \\ &\times \langle \psi_\alpha^{(-)}(\mathbf{q}_f) \nu_{\alpha_f}(Nd) | j^\mu(\mathbf{k}_\gamma, \mathbf{p}_N + \mathbf{p}_d + \mathbf{p}_B) \epsilon_\mu(\mathbf{k}_\gamma, \lambda) | B \rangle_{\mathbf{q}_f = \frac{\mathbf{p}_d - 2\mathbf{p}_N}{3}}, \end{aligned} \quad (2.14a)$$

from which the differential cross section

$$d\sigma^{dis} = \langle s_f | M^{dis} | s_i \rangle^2 \frac{dLips(k_\gamma + p_B, p_N, p_d)}{4c^2(p_B \cdot k_\gamma)}. \quad (2.14b)$$

is obtained. Its dependence on the helicity λ and on the spin projection \mathcal{M}_{B_i} of photon and trinucleon bound state in the initial channel, collectively described by s_i , and on the spin projections m_{s_f} and M_{I_f} of nucleon and deuteron in the final channel, collectively described by s_f , are explicitly indicated. $\langle s_f | M^{dis} | s_i \rangle$ is Lorentz-invariant and can be calculated in any frame. We choose the c.m. frame and follow the computational strategy of Sect. 2.2.1 for radiative capture:

- The experimental photon energy in the lab frame determines the total energy of the system and therefore the c.m. momentum \mathbf{k}_γ in the initial channel. This step is done using relativistic kinematics.
- All hadron energies involved in the matrix element (2.14a) are chosen nonrelativistically and consistent with their model values.

- Taking the computed trinucleon binding energy for calculating the rest mass m_B and the average nucleon mass for the nucleon mass m_N , i.e., $m_N c^2 = 938.919$ MeV, the relative momentum \mathbf{q}_f of the final nucleon-deuteron system is determined employing the nonrelativistic forms (2.6) for the hadron energies, i.e., $m_N c^2 + m_d c^2 + \mathbf{q}_f^2 / (4m_N/3) = |\mathbf{k}_\gamma c| + m_B c^2 + \mathbf{k}_\gamma^2 / 6m_N$. Since the model rest mass m_B is not the experimental one, neither for ${}^3\text{He}$ nor for ${}^3\text{H}$ reactions, that nucleon-deuteron energy does not have the experimental value.

The other building blocks for the differential cross section (2.14b) are the Lorentz-invariant phase-space element $dLips(k_\gamma + p_B, p_N, p_d)$, i.e.,

$$dLips(k_\gamma + p_B, p_N, p_d) = (2\pi\hbar)^4 \delta(k_\gamma + p_B - p_N - p_d) \frac{d^3 p_N}{(2\pi\hbar)^3 2E_N(\mathbf{p}_N)} \frac{d^3 p_d}{(2\pi\hbar)^3 2E_d(\mathbf{p}_d)}, \quad (2.15)$$

and the incoming flux $4c^2(p_B \cdot k_\gamma)$. In contrast to the matrix element $\langle s_f | M^{dis} | s_i \rangle$ which contains our model assumptions, the kinematic parts of the differential cross section, the Lorentz-invariant phase-space element and the incoming flux, have to be calculated with the true experimental and relativistic energies of nucleon, deuteron and trinucleon bound state. In the c.m. system the differential cross section takes the form

$$\left. \frac{d\sigma_{c.m.}^{dis}}{d^2 \hat{\mathbf{p}}_N} \right|_{s_i \rightarrow s_f} = \frac{1}{64\pi^2} \frac{1}{(\hbar c)^2} \left| \langle s_f | M^{dis} | s_i \rangle \right|^2 \frac{|\mathbf{p}_N|}{|\mathbf{k}_\gamma|} \frac{1}{(k_\gamma c + E_B(\mathbf{k}_\gamma))^2}. \quad (2.16a)$$

That form of the cross section still describes the transition between specified spin states. The spin-averaged differential cross section is

$$\overline{\left. \frac{d\sigma_{c.m.}^{dis}}{d^2 \hat{\mathbf{p}}_N} \right|_{s_i \rightarrow s_f}} = \frac{1}{4} \sum_{\lambda M_{B_i}} \sum_{M_{N_f} M_{d_f}} \left. \frac{d\sigma_{c.m.}^{dis}}{d^2 \hat{\mathbf{p}}_N} \right|_{s_i \rightarrow s_f}. \quad (2.16b)$$

The S -matrix of photo disintegration and radiative capture are related, due to time reversal, in corresponding kinematics situations $|\mathbf{k}_\gamma|c + E_B(\mathbf{p}_B) = E_N(\mathbf{p}_N) + E_d(\mathbf{p}_d)$, i.e., $|\langle f \mathbf{P}_f | S^{dis} | i \mathbf{P}_i \rangle| = |\langle f \mathbf{P}_f | S^{rc} | i \mathbf{P}_i \rangle|$, where the initial and final states of the matrix elements for photo disintegration and radiative capture are to be interchanged. That S -matrix relation is derived in Appendix A. As a consequence, the differential cross section of photo disintegration and radiative capture are obtained from each other by

$$\overline{\left. \frac{d\sigma_{c.m.}^{dis}}{d^2 \hat{\mathbf{p}}_N} \right|_{s_i \rightarrow s_f}} \left/ \overline{\left. \frac{d\sigma_{c.m.}^{rc}}{d^2 \hat{\mathbf{k}}_\gamma} \right|_{s_i \rightarrow s_f}} \right. = \frac{6}{4} \frac{|\mathbf{p}_N|^2}{|\mathbf{k}_\gamma|^2}. \quad (2.17)$$

2.2.3 Spin Observables

Spin observables are defined as in ref. [2]. In this paper we consider polarization in the nucleon-deuteron system only. Thus, analyzing powers A in radiative

capture are

$$A = \frac{\text{Tr}(M^{rc} S^a M^{rc\dagger})}{\text{Tr}(M^{rc} M^{rc\dagger})}. \quad (2.18)$$

The spin operators S^a refer to the nucleon, i.e., $S^a = \{\sigma_i\}$, or to the deuteron, i.e., $S^a = \{S_i, S_{jk}\}$; we take over the definitions of ref. [2]. For the deuteron analyzing powers the equivalent spherical tensor notation iT_{11} and T_{2m} will often be used as in ref. [2]. Details of the calculation of spin observables are also given in Appendix A.

3 Results

The results are based on calculations derived from the coupled-channel two-baryon potential A2 of ref. [16]. The potential is an extension of the purely nucleonic Paris potential [17] extended in isospin-triplet partial waves for single Δ -isobar excitation. The Δ -isobar is considered to be a stable particle of spin and isospin 3/2 with a rest mass $m_\Delta c^2$ of 1232 MeV. The extension is almost phase-equivalent [18, 19] to the underlying nucleonic potential. The potential is used in the separably expanded form of ref. [1]. Partial waves up to total pair angular momentum $I = 2$ are taken into account.

The AGS three-particle equations for the trinucleon bound state $|B\rangle$ are solved as in ref. [1]. The resulting binding energy $m_B c^2 - 3m_N c^2$ is -7.702 MeV for the coupled-channel potential A2 and -7.373 MeV for the Paris potential, the purely nucleonic reference potential. If the Coulomb interaction is taken into account, as proper for ${}^3\text{He}$, the binding energies shift to -7.033 MeV and -6.716 MeV; the e.m. shifts are calculated perturbatively in ref. [20], amounting to 669 keV for a coupled-channel potential with Δ -isobar excitation and to 657 keV for the purely nucleonic reference potential. Nevertheless, we use the purely hadronic values -7.702 MeV and -7.373 MeV as model values for calculating the matrix elements (2.11b) and (2.14a) of the considered photo reactions, since the calculation leaves out e.m. effects in the hadronic wave functions. For ${}^3\text{He}$, as needed in most described reactions, they differ slightly from the experimental value -7.718 MeV. We shall describe proton-deuteron radiative capture for the two deuteron lab energies 19.8 MeV and 95 MeV; according to our calculational strategy, the photon energies in the final states are 12.05 (11.72) MeV and 36.97 (36.65) MeV for the theoretical binding energy of ${}^3\text{He}$ with (without) Δ -isobar, the discrepancy with the values 12.07 MeV and 36.99 MeV arising from the experimental ${}^3\text{He}$ binding energy is quite small. The wave function of the bound state is expanded in terms of the $(\mathcal{L}S)$ coupled basis states defined in Appendix B.1; the expansion is done according to Appendix B.2; the infinite expansion is first truncated to include all states up to total pair angular momentum $I = 6$ in (Ij) coupling and then transformed to $(\mathcal{L}S)$ coupling. The convergence of the presented results with respect to that truncation is checked and found to be satisfactory for all reactions corresponding to deuteron lab energies between 1 and 100 MeV: Additional wave function components usually change observables by less than 0.1% in the complete kinematic regime with the exception of sensitive spin observables with values close to zero: They may change within 1%.

The AGS three-particle equations for the nucleon-deuteron scattering states $|\psi_\alpha^{(\pm)}(\mathbf{q})\nu_\alpha(Nd)\rangle$ are solved as in ref. [4]; in contrast to ref. [2], ref. [4] uses real-axis integration for the solution. The wave functions are expanded in terms of the (Ij) coupled states defined in Appendix B.1; the terms of the infinite expansion according to Appendix B.3, contributing to the matrix element $\langle\psi_\alpha^{(-)}(\mathbf{q}_f)\nu_{\alpha_f}(Nd)|j^\mu(\mathbf{k}_\gamma, \mathbf{p}_N + \mathbf{p}_d + \mathbf{p}_B)\epsilon_\mu(\mathbf{k}_\gamma\lambda)|B\rangle$ of photo disintegration, are limited with respect to total three-particle angular momentum \mathcal{J} and with re-

spect to total pair angular momentum I by the angular momenta contained in the trinucleon bound-state wave function and in the considered current multipoles. We note that also for radiative capture that matrix element of photo disintegration is calculated and time reversal is employed according to Appendix A.

The e.m. current is taken over from ref. [12]. Certain coupling constants, especially those referring to the Δ -isobar, are not up-to-date anymore; nevertheless, we decided not to change them in the present paper in order to preserve a valuable historic continuity with our past calculations [12, 15, 21] for related observables. The technique for calculating multipole matrix elements is developed in refs. [22, 23]; a special stability problem arising in the calculation is discussed in Appendix B.5. Our calculation for photo processes with internal excitation energies of the three-nucleon system up to 50 MeV includes electric and magnetic dipole and quadrupole contributions, abbreviated in an obvious way by $E1$, $E2$, $M1$ and $M2$. The magnetic multipoles are calculated according to Eq. (B.12b) of Appendix B.4 from the one- and two-baryon parts of the current. The electric multipoles are calculated in the Siegert form according to Eq. (B.13a) of Appendix B.4. The first term of Eq. (B.13a) is calculated from the one- and two-baryon parts of the current. The second term of Eq. (B.13a) is the physically much more important proper Siegert term; it is replaced by model energies and Coulomb multipoles; the contributing charge density has diagonal single-nucleon and single- Δ contributions only; the nucleon- Δ transition contribution as well as two-baryon contributions are of relativistic order and are therefore omitted in the charge-density operator when calculating Coulomb multipoles.

3.1 *Calculational Tests*

3.1.1 Test of the Employed E.M. Current

As test of the employed e.m. current operator the magnetic form factors F_M of the trinucleon bound state are calculated. In fact, the obtained results are recalculations of our previous ones given in refs. [12, 15, 21] with updated techniques; they are shown in Figs. 6 and 7 individually for ${}^3\text{He}$ and ${}^3\text{H}$ and for their isospin-separated parts. Concerning the bound-state wave function, more mesh points and channels are included in the present calculation, significantly improving the results in and beyond the first diffraction minimum technically. Concerning the e.m. current, a sign mistake got detected in the two-baryon transition current from nucleonic to nucleon- Δ states; that contribution is in general very small, but becomes significant when all other contributions cancel, i.e., in the region of the diffraction minimum. Both effects combined, the one arising from the improved bound-state wave function and the other arising from a corrected two-baryon transition current, yield changes in the magnetic form factors at momentum transfer $Q > 4 \text{ fm}^{-1}$, decreasing the weight of the Δ -isobar for the magnetic form factors somehow, compared with the results of ref. [21].

3.1.2 Test of the Calculational Apparatus for Radiative Capture

A detailed comparison of the calculational procedure of this paper and of the one in refs. [7, 8] is carried out. The comparison is done for a purely nucleonic calculation and with a heavily truncated potential; only the two partial waves 1S_0 and $^3S_1 - ^3D_1$ are kept and the separable expansion is simplified to include three and four terms only, i.e., it is of rank 3 and 4, respectively. With respect to the current, only the $E1$ multipole is employed in the long-wave length form $T_{elec\ m_1}^{(1,l.w.)}(k_\gamma/\hbar)$ according to Eq. (B.15b). Furthermore, the choice of momenta and energies for the current matrix element follows refs. [7, 8] in the rest of this subsection and not our own computational strategy as discussed in Subsect. 2.2. With the stated choice, the conceptual differences between the two calculations should be minimal and a detailed comparison is meaningful. On the other hand, the practical difference between the two calculations is enormous, especially with respect to the treatment of the permutation operator.

The achieved agreement between the calculations of refs. [7, 8] and of this paper is quite satisfactory. We have compared the differential cross section and spin observables iT_{11} , T_{20} , T_{21} , T_{22} and A_{yy} . Fig. 8 shows characteristic results. For 10 MeV we show the case of poorest agreement, for other observables the results of both calculations are not distinguishable in a plot. For 45 MeV we also show the poorest case of agreement; the differential cross section and T_{22} have similar discrepancies, while the other observables are often not distinguishable in a plot. We conclude that our code for calculating trinucleon photo reactions is numerically quite reliable.

3.1.3 Multipole Expansion of Current

Our full calculations are based on a coupled-channel two-baryon potential with single Δ -isobar excitation and on a corresponding e.m. current with the same coupling. The current is expanded into electric and magnetic multipoles. The convergence of results due to that multipole expansion of the current is studied in this subsection.

The first study is carried out for the full calculations of radiative capture with Δ -isobar excitation; the results for spin-averaged differential cross sections and for the spin observable A_{yy} for 95 MeV, the highest considered deuteron lab energy, are shown in Fig. 9. The electric dipole operator of the Siegert form, i.e., the second term in Eq. (B.13a) for $E1$, makes a significant contribution to most observables in the studied energy range. The first term of Eq. (B.13a) for $E1$ is unimportant for the differential cross section, but sizeable for spin observables; this observed fact is not documented in Fig. 9. The expansion with respect to the considered multipoles, i.e., multipoles up to $E2$ and $M2$, appears well converged. The contributions from the $E3$ and $M3$ multipoles, calculated tentatively, turn out to be very small for all observables, as is shown in Fig. 9.

In Fig. 10 the multipole expansion is studied for the energy dependence of the two spin observables A_{yy} and T_{20} at 90° lab scattering angle of the proton. The study is carried out for calculations with the purely nucleonic reference

potential. Up to 30 MeV deuteron lab energy the electric dipole operator $E1$ in the Siegert form, i.e., the second term of Eq. (B.13a), determines the observables; in fact, its long-wavelength limit form Eq. (B.15b) suffices. Beyond 30 MeV the first term in Eq. (B.13a) for $E1$ and the $M1$ and $M2$ multipoles become significant, but they tend to cancel each other; this fact, which we consider a non-understood coincidence, makes the result based on the $E1$ operator in Siegert form close to the full result. The contributions of $E2$ and higher electric or magnetic multipoles remain small. In comparison with ref. [8] we note in passing that beyond 30 MeV deuteron lab energy also the improved hadronic interaction with respect to high partial waves and additional ranks in the separable expansion gives rise to rather sizeable changes.

3.1.4 Frame Independence of Matrix Elements $\langle s_f | M^{rc} | s_i \rangle$ and $\langle s_f | M^{dis} | s_i \rangle$ in Eqs. (2.11b) and (2.14a)

The current matrix elements $\langle s_f | M^{rc} | s_i \rangle$ and $\langle s_f | M^{dis} | s_i \rangle$ are conceptionally Lorentz-invariant scalars and could therefore be calculated in any frame with identical results. We choose the c.m. frame for calculations of this paper. However, our calculational apparatus does not strictly respect Lorentz invariance, the results are frame-dependent. We therefore check that possible frame dependence of results and alternatively calculate the same current matrix elements also in the lab system. We do so for two-body photo disintegration at 36.9 MeV c.m. photon energy, i.e., for the matrix elements $\langle s_f | M^{dis} | s_i \rangle$. The recalculation in the lab system uses the initial lab photon momentum \mathbf{k}_γ and requires the redetermination of relative momentum \mathbf{q}_f of the final nucleon-deuteron system employing the nonrelativistic forms (2.6) for the hadron energies, i.e., $m_N c^2 + m_d c^2 + \mathbf{q}_f^2 / (4m_N/3) + \mathbf{k}_\gamma^2 / 6m_N = |\mathbf{k}_\gamma c| + m_B c^2$. The current operator needed for calculating the S -matrix element $\langle s_f | M^{dis} | s_i \rangle$ is of nonrelativistic order; it has the same functional form as for the calculation in the c.m. system, except for the single-baryon convection current.

The $E1$ contribution to the matrix element $\langle s_f | M^{dis} | s_i \rangle$ is calculated according to Eq. (B.14a), the $E2$ contribution according to Eq. (B.12a) and $M1$ and $M2$ contributions according to Eq. (B.12b). Especially the two individual terms of the $E1$ contribution show a frame dependence of the order 2%; however, that frame dependence cancels out for the sum of all multipoles considered. Resulting observables of two-body photo disintegration at 36.9 MeV c.m. energy are frame-independent up to a level of 0.01%. Thus, we conclude that all matrix elements $\langle s_f | M^{rc} | s_i \rangle$ and $\langle s_f | M^{dis} | s_i \rangle$, calculated in this paper, are sufficiently frame-independent.

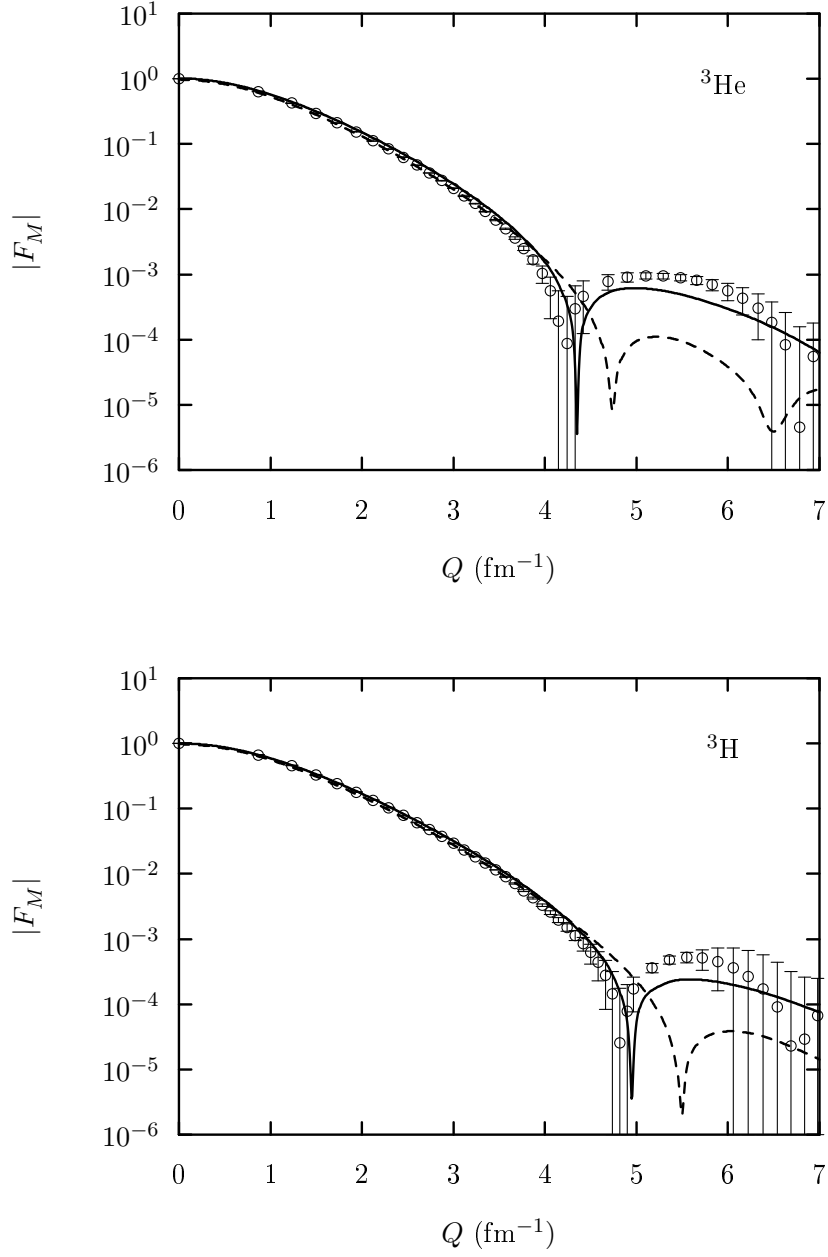


Figure 6. Magnetic form factors F_M of ${}^3\text{He}$ and ${}^3\text{H}$ as function of momentum transfer Q . The results for the interaction with Δ -isobar excitation are shown as solid lines, whereas the results for the purely nucleonic reference potential, the Paris potential, are shown as dashed lines. The experimental data are taken from ref. [24]

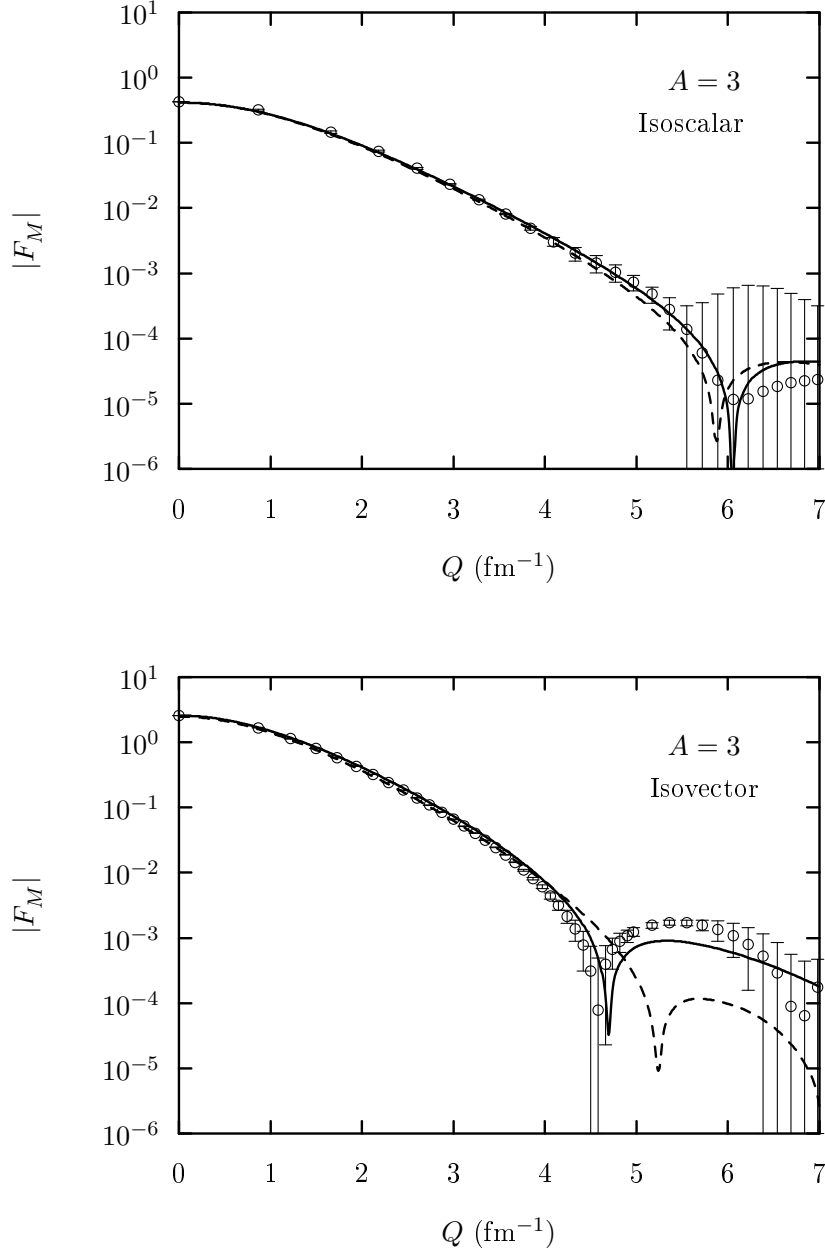


Figure 7. Isoscalar and isovector trinucleon magnetic form factors F_M as function of momentum transfer Q . The results for the interaction with Δ -isobar excitation are shown as solid lines, whereas the results for the purely nucleonic reference potential, the Paris potential, are shown as dashed lines. The experimental data are taken from ref. [24]

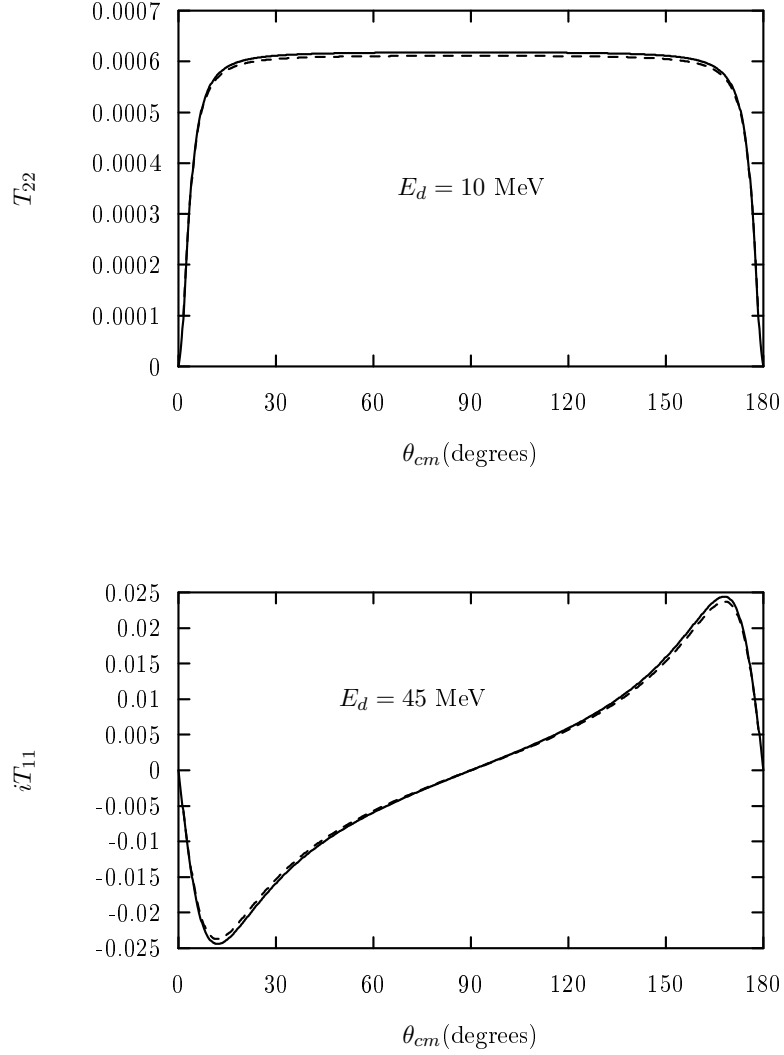


Figure 8. Comparison of the computational procedure of this paper with the one of refs. [7, 8]. The comparison uses the two spin observables T_{22} and iT_{11} of radiative capture at 10 MeV and 45 MeV deuteron lab energies, respectively. The scattering angle θ_{cm} is the c.m. scattering angle of the photon with respect to the direction of the proton. The results use a simplified dynamics for the hadronic and e.m. interactions as described in Subsect. 3.1.2. The results based on the technique of this paper are shown as solid lines, the ones based on the technique of refs. [7, 8] as dashed lines.

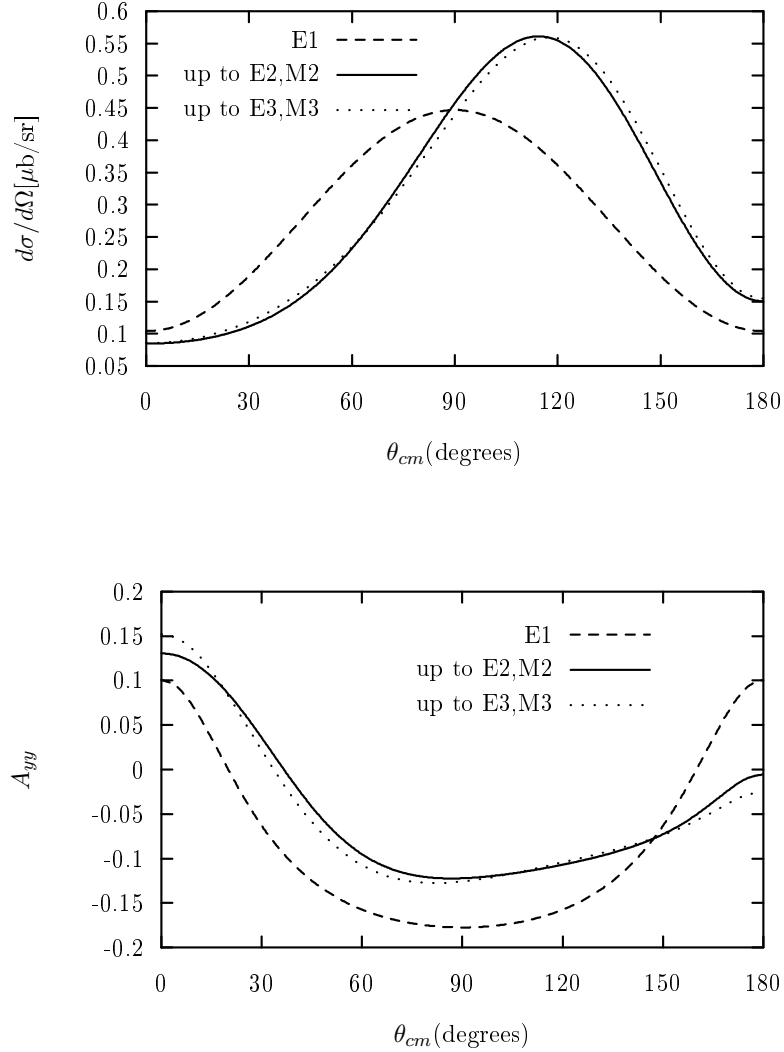


Figure 9. Convergence of the multipole expansion of the e.m. current. The differential cross section and the spin observable A_{yy} are sample observables. Contributions from multipole up to $E3, M3$ are presented for radiative capture at 95 MeV deuteron lab energy as function of the c.m. scattering angle of the photon with respect to the direction of the deuteron; the $E1$ contributions include both terms of Eq. (B.13a). The results refer to full calculations with Δ -isobar excitation.

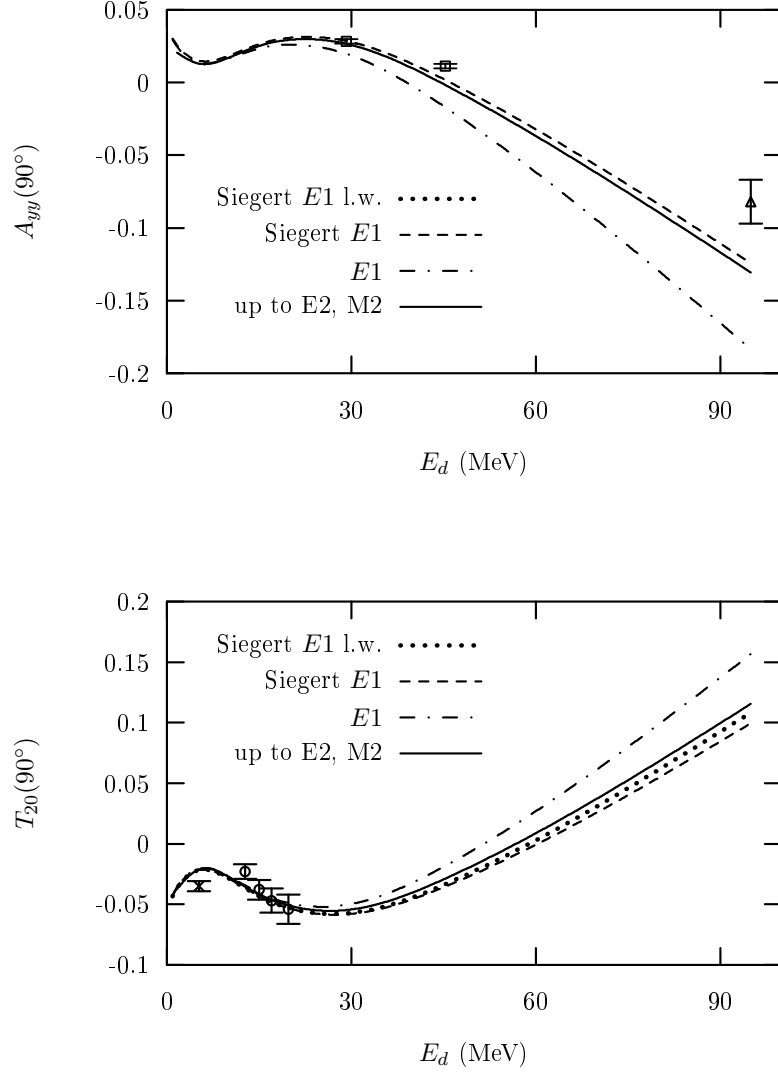


Figure 10. Spin observables of radiative capture at 90° lab scattering angle of the proton with respect to the direction of photon as function of deuteron lab energy. A_{yy} is shown in the top, where the experimental data come from refs. [28] (open squares) and [27] (upper triangle); T_{20} is shown in the bottom, where the experimental data come from refs. [29] (open circles) and [30] (cross). The results refer to calculations with the purely nucleonic reference potential. For the solid curves all multipoles up to $E2$, $M2$ are included, for the dashed curves only $E1$ in the Siegert form of term two in Eq. (B.13a), for the dotted curves its long-wavelength limit according to Eq. (B.15b) and for the dashed-dotted curves $E1$ with both terms in Eq. (B.13a). In the top the solid and dotted curves are indistinguishable and are therefore not drawn separately.

3.2 Physics Results

3.2.1 Δ -Isobar Effects in Radiative Capture

This subsection presents full results for radiative capture. They are compared with those of a purely nucleonic reference calculation without Δ -isobar excitation which are derived from a purely nucleonic potential and a purely nucleonic current; the Paris potential is the nucleonic reference potential.

First, in Figs. 11 and 12 we give sample results for 19.8 MeV and 95 MeV deuteron lab energies. In the figures we follow the standard convention for the presentation of data as introduced in refs. [25–27]: At 19.8 MeV the c.m. photon angle refers to the direction of the proton, i.e., it is the c.m. ${}^3\text{He}$ angle with respect to the deuteron direction; at 95 MeV the c.m. photon angle refers to the direction of the deuteron.

The total Δ -isobar effect is for all considered observables rather moderate. The inclusion of the Δ -isobar does not change the phase-space or flux contributions to the cross sections, they are purely nucleonic and are given by the experimental conditions. However, the inclusion of the Δ -isobar changes the current matrix element; its change can arise from four different sources:

- The inclusion of the Δ -isobar changes the theoretical trinucleon binding energy and thereby changes the theoretical photon energy of the process.
- The inclusion of the Δ -isobar adds Δ -components to the bound-state wave function and alters its nucleonic ones.
- The inclusion of the Δ -isobar adds Δ -components to the wave function of the nucleon-deuteron scattering state and alters its nucleonic ones.
- The inclusion of the Δ -isobar adds current components which couple to Δ -components in the hadronic wave functions.

Figs. 13 and 14 try to distinguish the respective importance of those Δ -isobar effects. The figures demonstrate that at the lower energy the Δ -isobar effects come mainly from changes in the binding energy and wave function of the bound state, at the higher energy mainly from the scattering state and the Δ -components of the e.m. current.

Second, Fig. 15 shows results for selected observables, i.e., A_{yy} and T_{20} at 90° lab scattering angle of the proton, as function of deuteron lab energy, the Δ -isobar effect is small. We remind the reader that in Fig. 10 the multipole expansion is discussed for both observables. It is a physically remarkable effect, proven there, that below 30 MeV deuteron lab energy both observables are determined by the $E1$ Siegert operator of Eq. (B.15b) of the long-wavelength limit in a model-independent way. In fact, the contribution of that simple operator describes the whole energy regime considered extremely well, but that result is above 30 MeV deuteron lab energy due to a cancellation of rather sizeable other contributions arising from the first term of the $E1$ operator in Eq. (B.13a) and from other electric and magnetic multipoles.

In conclusion, we have theoretical predictions for existing experimental data in the whole considered energy domain. However, we refrain from showing more results; they are available from the authors upon request.

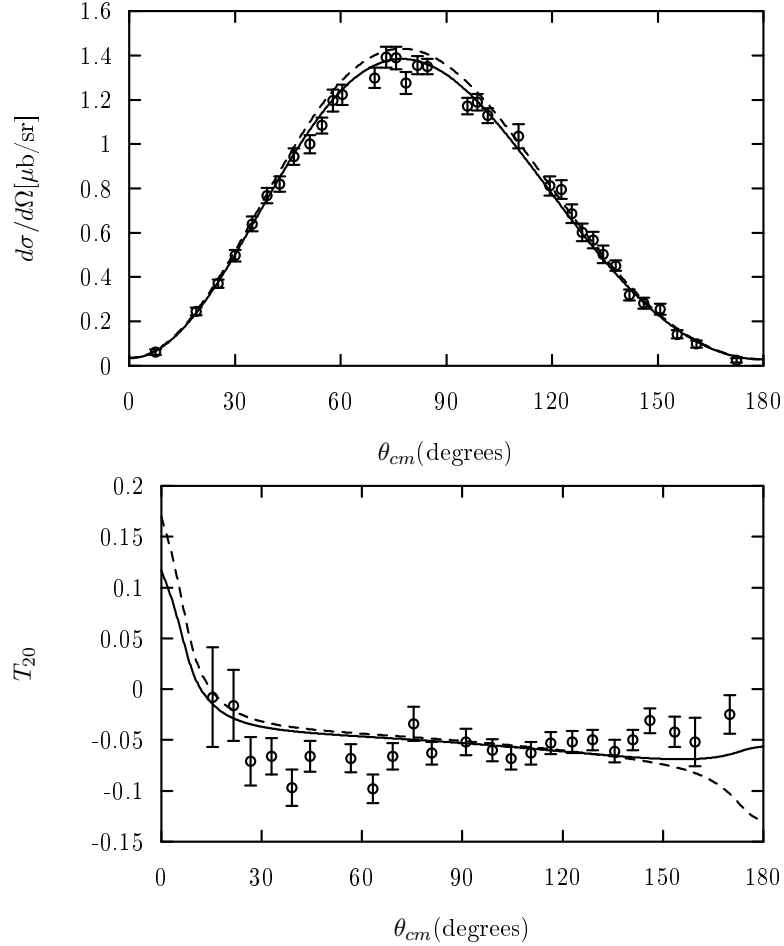


Figure 11. Radiative capture at 19.8 MeV deuteron lab energy as function of the c.m. scattering angle of the photon with respect to the direction of the proton. The differential cross section is shown on the top; the experimental data are taken from ref. [25]. The spin observable T_{20} is shown on the bottom; the experimental data are taken from ref. [26]. The full results for the interaction with Δ -isobar excitation are shown as solid lines, whereas the results for the purely nucleonic reference potential, the Paris potential, are shown as dashed lines.

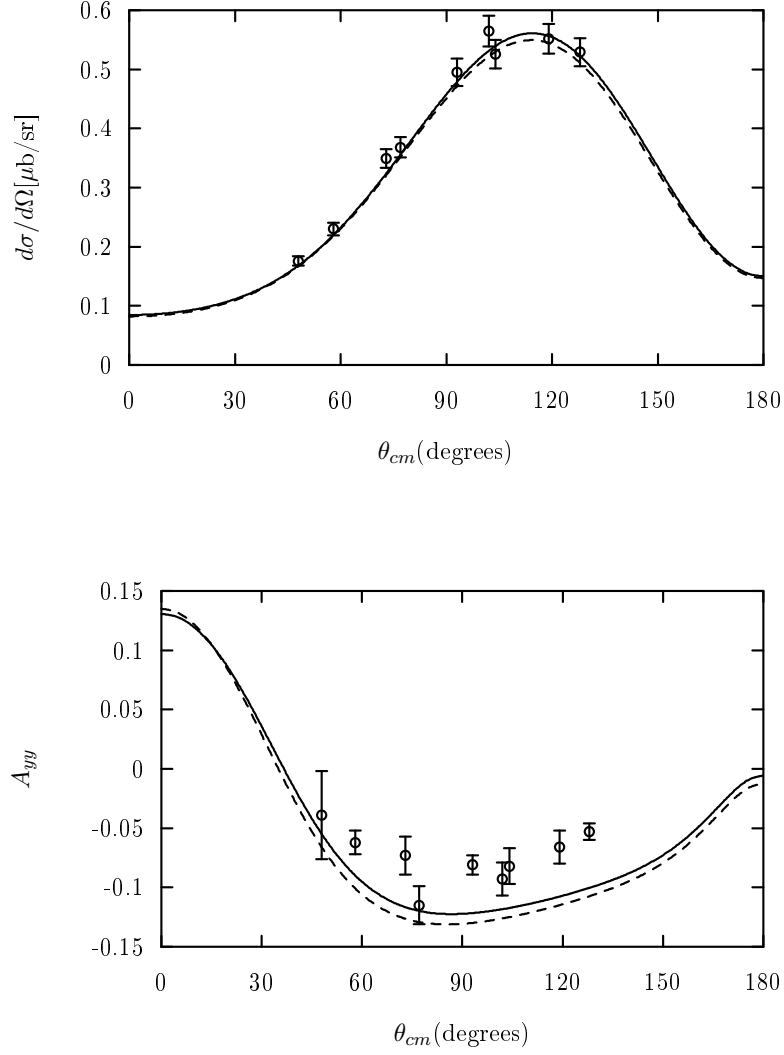


Figure 12. Radiative capture at 95 MeV deuteron lab energy as function of the c.m. scattering angle of the photon with respect to the direction of the deuteron. The differential cross section is shown on the top. The spin observable A_{yy} is shown on the bottom; both sets of experimental data are taken from ref. [27]. The full results for the interaction with Δ -isobar excitation are shown as solid lines, whereas the results for the purely nucleonic reference potential, the Paris potential, are shown as dashed lines.

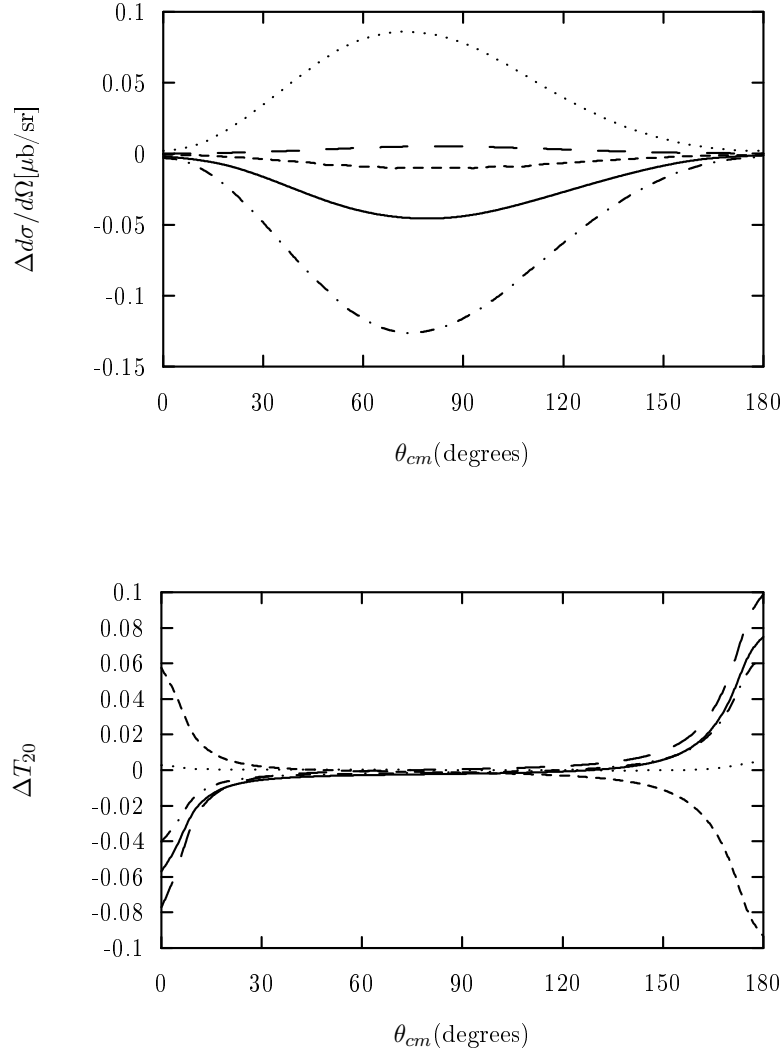


Figure 13. Contributions to the Δ -isobar effect for radiative capture at 19.8 MeV deuteron lab energy as function of the c.m. scattering angle of the photon with respect to the direction of the proton. The c.m. differential cross section is shown on the top; the spin observable T_{20} on the bottom. Shifts in the observables are shown. The full shift in the prediction arising from the different predictions of the nucleonic reference potential and the coupled-channel potential is shown as solid lines. That full shift is split up into four parts, i.e., the contribution arising from the theoretical change of the triton binding energy due to scaling (dotted lines), the contribution arising from the change of the nucleonic components of the bound wave function (dashed-dotted lines), the contribution arising from the change of the nucleonic components of the scattering function (short-dashed lines), and the contribution arising from the Δ -components in both baryonic wave functions and the e.m. current (long-dashed lines); those four contributions add up to the full shift making up the complete Δ -isobar effect.

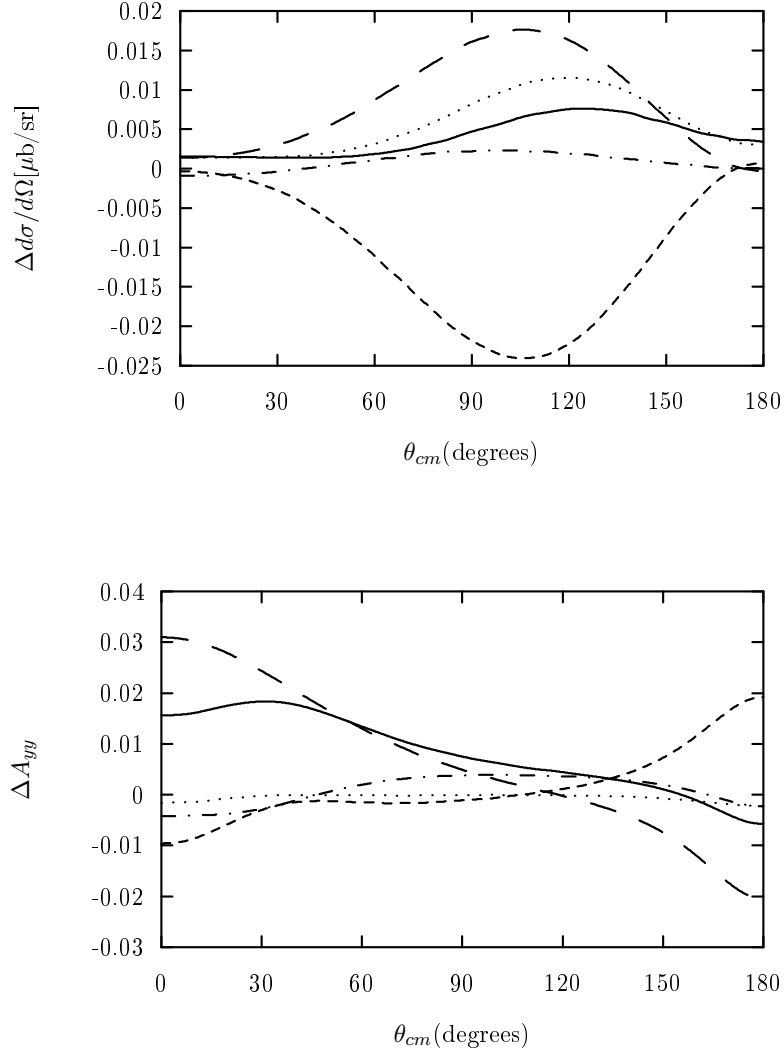


Figure 14. Contributions to the Δ -isobar effect for radiative capture at 95 MeV deuteron lab energy as function of the c.m. scattering angle of the photon with respect to the direction of the deuteron. The differential cross section is shown on the top; the spin observable A_{yy} is shown on the bottom. Shifts in the observables are shown. The meaning of the different types of lines is the same as in Fig. 13.

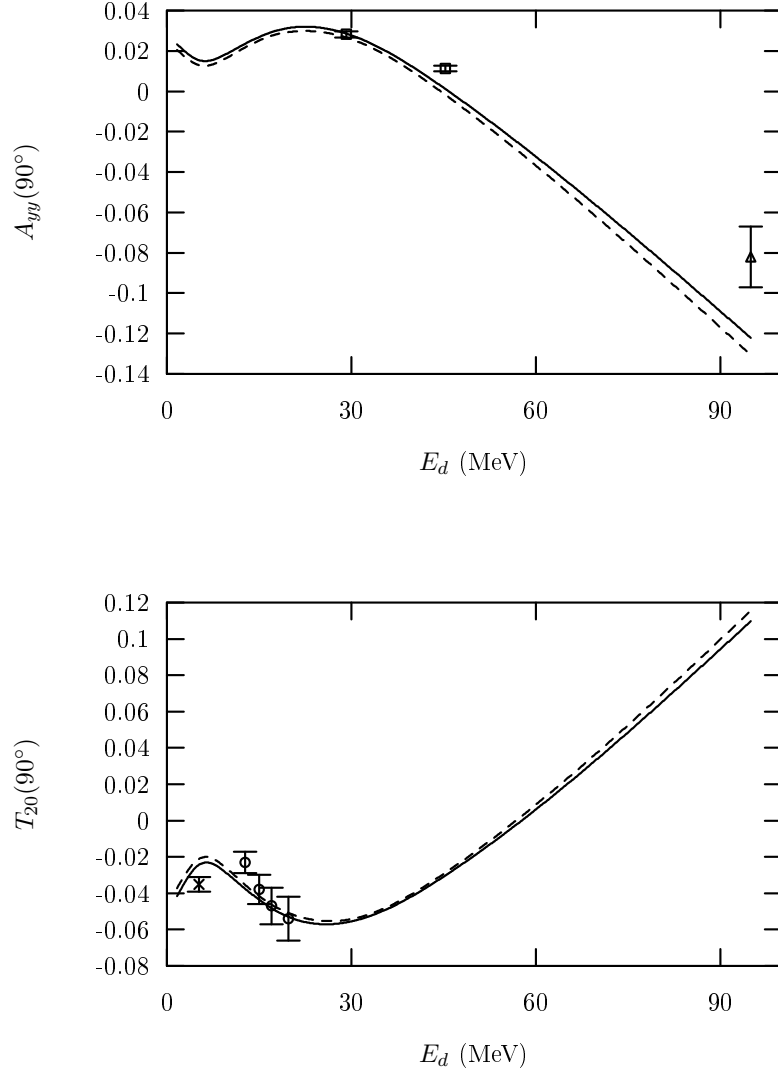


Figure 15. Spin observables of radiative capture at 90° lab scattering angle of the proton with respect to the direction of photon as function of deuteron lab energy. A_{yy} is shown in the top, where the experimental data come from refs. [28] (open squares) and [27] (upper triangle); T_{20} is shown in the bottom, where the experimental data come from refs. [29] (open circles) and [30] (cross). The results for the full interaction with Δ -isobar excitation are shown as solid lines, whereas the results for the purely nucleonic reference potential, the Paris potential, are shown as dashed lines.

3.2.2 Results for Two-Body Photo Disintegration

According to Eq. (2.17) the cross sections for photo disintegration and radiative capture are simply related. In fact, the experimental data as shown in the figures of this subsection are taken from radiative capture; 12.2 (36.9) MeV photon c.m. energy corresponds to 19.8 (95.0) MeV deuteron lab energy of radiative capture.

The relation of Eq. (2.17) holds due to time reversal relation between experimental cross sections. Of course, time reversal relation remains true also for the matrix elements M^{dis} and M^{rc} of the model calculations, however, the meaning of kinematic correspondence is different in model calculations. We voted to always determine the initial c.m. momentum from the experimental lab energy by relativistic kinematics using experimental rest masses; the final c.m. momentum and energy are then determined by energy conservation using the nonrelativistic kinematics of the model calculation. Thus, the kinematics of the final state does not match properly the experimental situation. Our recipe, which is created by the fact that the model calculation is based on nonrelativistic quantum mechanics and is unable to reproduce the ${}^3\text{He}$ binding precisely, clearly creates a conceptual uncertainty, the magnitude of which this subsection tries to estimate.

We therefore calculated the spin-average differential cross section of ${}^3\text{He}$ two-body photo disintegration in two ways. In the first way, the experimentally corresponding radiative capture process is calculated and Eq. (2.17) is employed for the step to two-body photo disintegration. In the second way, two-body photo disintegration is calculated directly according to the procedure of Subsect. 2.2.2. The results are compared in Figs. 16 and 17 for a purely nucleonic reference calculation, since the purely nucleonic reference calculation misses the ${}^3\text{He}$ binding most and therefore should show the largest differences between the two calculational procedures. The complete Δ -isobar effect is also given in order to set the scale for the conceptual uncertainty of these calculations. Results are shown for 12.2 MeV and 36.9 MeV photon c.m. energies. Compared with the moderate complete Δ -isobar effect the conceptual uncertainty is small at the larger photon energy, but sizable at the small one.

In Fig. 18 we show the energy dependence of the lab differential cross section for triton two-body photo disintegration with two-body break-up at 90° lab scattering angle of the nucleon with respect to the direction of the photon.

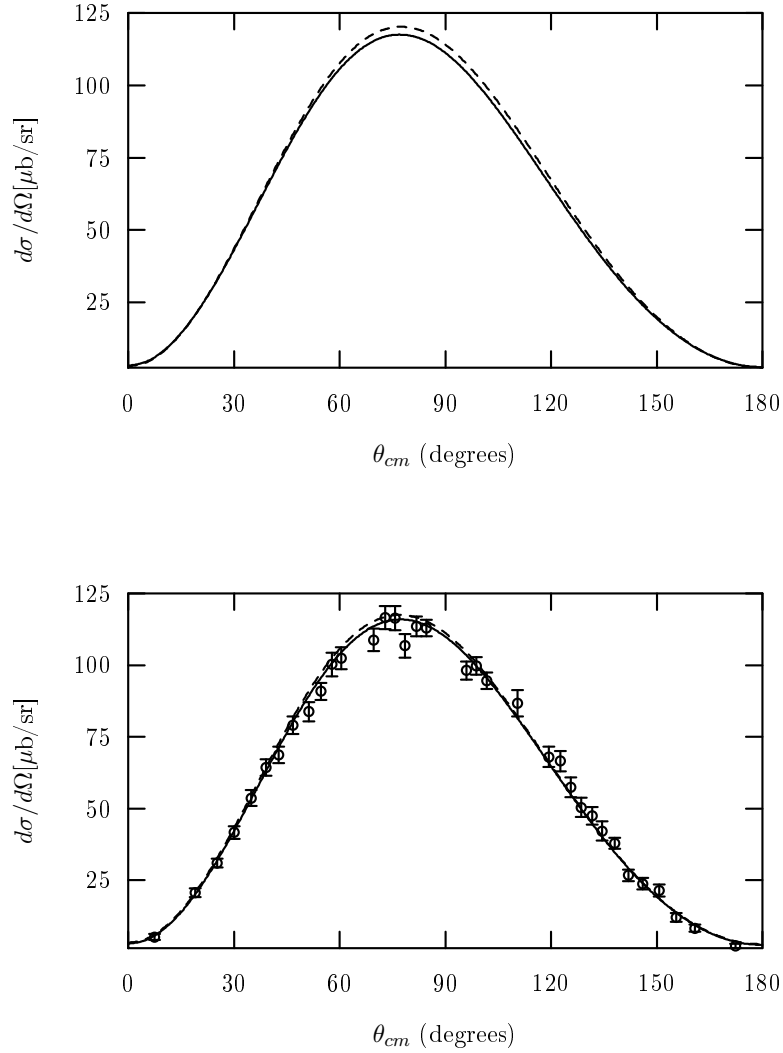


Figure 16. C.M. differential cross section of ${}^3\text{He}$ photo disintegration with two-body break-up at 12.2 MeV photon c.m. energy as function of the c.m. scattering angle of the proton with respect to the direction of the photon. (a) In the upper part, the results of computational methods based on detailed balance according to Eq. (2.17) and on the procedure of Subsect. 2.2.2, are compared by the dashed line and the solid line, respectively. The results refer to a purely nucleon reference calculation. (b) In the lower part of the figure, the complete Δ -isobar effect is shown; here the calculations use the procedure of Subsect. 2.2.2. The full result for the coupled-channel interaction with Δ -isobar excitation is given by the solid line, the purely nucleonic reference result by the dashed line.

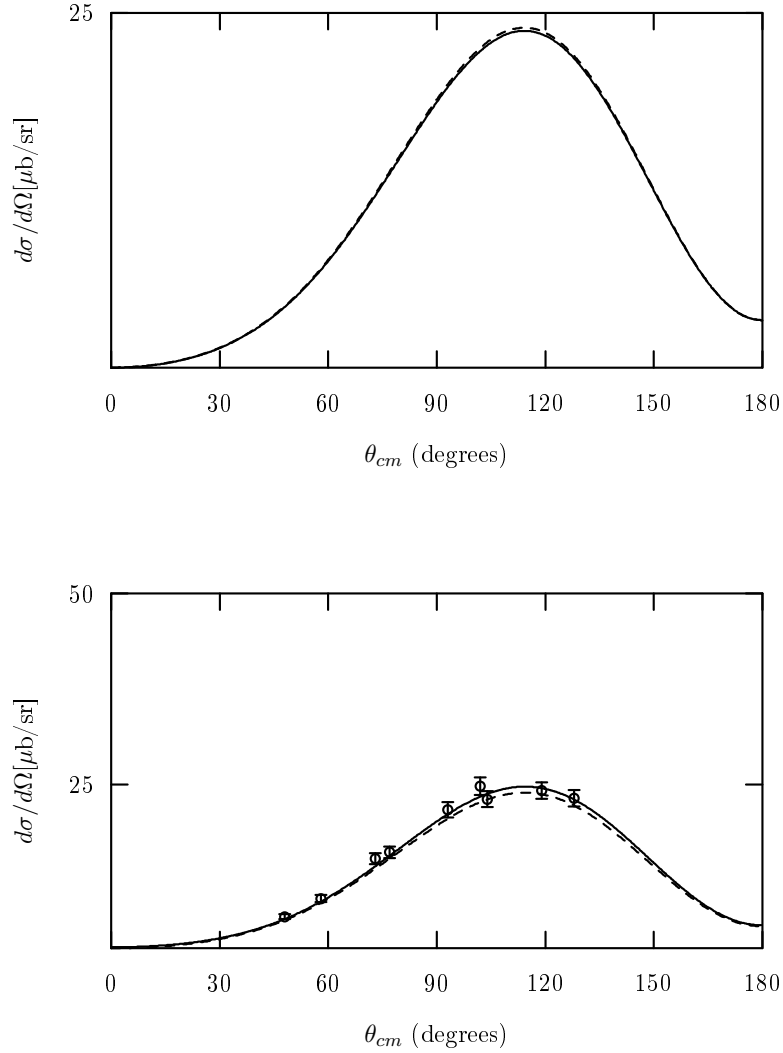


Figure 17. C.M. differential cross section of ${}^3\text{He}$ photo disintegration with two-body break-up at 36.9 MeV photon c.m. energy as function of the c.m. scattering angle of the deuteron with respect to the direction of the photon. (a) In the upper part, the results of computational methods based on detailed balance according to Eq. (2.17) and on the procedure of Subsect. 2.2.2, are compared by the dashed line and the solid line, respectively. The results refer to a purely nucleon reference calculation. (b) In the lower part of the figure, the complete Δ -isobar effect is shown; here the calculations use the procedure of Subsect. 2.2.2. The full result for the coupled-channel interaction with Δ -isobar excitation is given by the solid line, the purely nucleonic reference result by the dashed line.

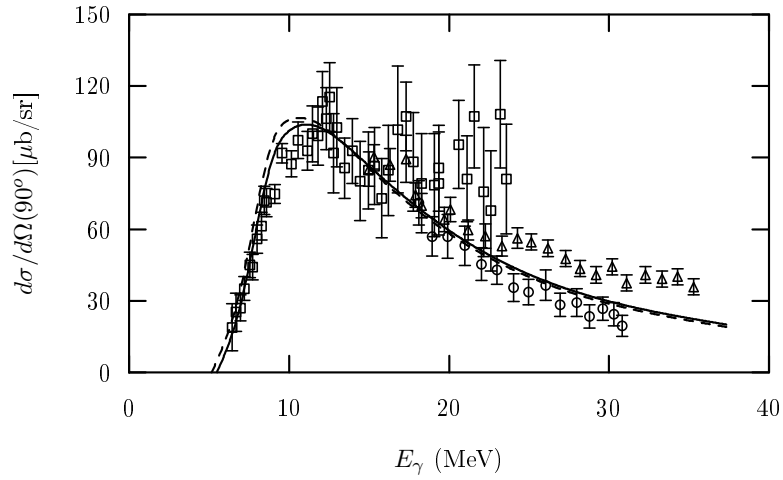


Figure 18. Lab differential cross section for ${}^3\text{H}$ photo disintegration with two-body break-up as function of the photon lab energy. The results refer to 90° nucleon lab angle with respect to the direction of the photon. The results of the full calculations with Δ -isobar excitation are shown as solid lines, those of the reference calculations without Δ -isobar excitation as dashed lines. Experimental data are taken from refs. [31] (open circles), [32] (open squares), and [33] (upper triangles).

4 Conclusion

The paper calculates radiative nucleon-deuteron capture for selected energies and compares the theoretical predictions with existing proton-deuteron data. Some results for two-body photo disintegration are also given. The calculation includes the Δ -isobar in the hadronic and the e.m. interactions. It employs fully correlated hadronic states and an e.m. current consisting of one-baryon and two-baryon contributions.

The Δ -isobar effect is isolated; it is moderate. At lower energies, it is mainly due to the shift in triton binding energy and due to the corresponding change in the nucleonic components of the bound-state wave function, brought about by the presence of the Δ -isobar. It is also found that below 30 MeV deuteron lab energy the spin observables A_{yy} and T_{20} at 90° lab scattering angle can be obtained model-independently from the $E1$ Siegert term in the long-wavelength limit. At higher energies, the Δ -isobar effect arises dominantly from the changes in the scattering wave function and in the e.m. current due to the Δ -isobar.

Acknowledgement. L. P. Yuan is supported in part by the DFG grant Sa 247/19-1 and by a graduate-student grant of Lower Saxony, M. Oelsner by the DFG grant Sa 247/20-1/2. J. Adam Jr. is supported by the grant GA CR 202/00/1669. The authors are grateful to Th. Wilbois for important help with the technical apparatus at the beginning of this work. The calculations are performed at Regionales Rechenzentrum für Niedersachsen.

Appendix A. Calculation of Amplitude

In Subjects. 2.2.1 and 2.2.2 the calculation of cross sections for nucleon-deuteron radiative capture and of two-body photo disintegration of the three-nucleon bound state is described. Both reactions are related by time reversal \mathcal{T} . We use in Subjects. 2.2.1 and 2.2.2 the same notation for the momenta of both reactions, though they are in fact different, i.e.,

$$\mathcal{T}|\mathbf{p}_N^{rc}\rangle = |(-\mathbf{p}_N^{rc})\rangle = |\mathbf{p}_N^{dis}\rangle , \quad (\text{A.1a})$$

$$\mathcal{T}|\mathbf{p}_d^{rc}\rangle = |(-\mathbf{p}_d^{rc})\rangle = |\mathbf{p}_d^{dis}\rangle , \quad (\text{A.1b})$$

$$\mathcal{T}|\mathbf{k}_\gamma^{rc}\rangle = |(-\mathbf{k}_\gamma^{rc})\rangle = |\mathbf{k}_\gamma^{dis}\rangle , \quad (\text{A.1c})$$

$$\mathcal{T}|\mathbf{p}_B^{rc}\rangle = |(-\mathbf{p}_B^{rc})\rangle = |\mathbf{p}_B^{dis}\rangle . \quad (\text{A.1d})$$

In this appendix we make the difference between the momenta of both reactions notationally explicit by the superscripts *rc* and *dis*. Time-reversal also changes angular momentum eigenstates $|jm\rangle$ by $\mathcal{T}|jm\rangle = (-1)^{j+m}|j(-m)\rangle$. Furthermore, the spin quantization axis, chosen in the experimental set-ups for the definition of spin observables, are different in both reactions. Fig. A.1 illustrates the kinematic situations of both reactions related by time reversal.

The current matrix element of radiative capture is obtained from the corresponding one of disintegration; the transverse helicities of the real photon are easier implemented in the disintegration matrix element choosing the direction of the incoming photon as z-direction.

$$\begin{aligned} & \langle B\mathcal{M}_B | j^\mu(-\mathbf{k}_\gamma^{rc}, \mathbf{p}_B^{rc} + \mathbf{p}_N^{rc} + \mathbf{p}_d^{rc}) \epsilon_\mu^*(\mathbf{k}_\gamma^{rc} \lambda) | \psi_\alpha^{(+)}(\mathbf{q}^{rc}) \nu_\alpha M_I m_s(Nd) \rangle \\ &= (-)^{\frac{1}{2} + \mathcal{M}_B} (-)^{1 + M_I} (-)^{\frac{1}{2} + m_s} \\ & \times \langle \psi_\alpha^{(-)}(\mathbf{q}^{dis}) \nu_\alpha(-M_I)(-m_s)(Nd) | j^\mu(\mathbf{k}_\gamma^{dis}, \mathbf{p}_N^{dis} + \mathbf{p}_d^{dis} + \mathbf{p}_B^{dis}) \epsilon_\mu(\mathbf{k}_\gamma^{dis} \lambda) | B(-\mathcal{M}_B) \rangle. \end{aligned} \quad (\text{A.2})$$

The derivation of Eq. (A.2) uses the general properties of current and photon-field operators under time reversal, i.e.,

$$\mathcal{T}J^\mu(x)\mathcal{T}^{-1} = J_\mu(\mathcal{T}x) , \quad (\text{A.3a})$$

$$\mathcal{T}A^\mu(x)\mathcal{T}^{-1} = A_\mu(\mathcal{T}x) , \quad (\text{A.3b})$$

and the condition

$$\epsilon^{*\mu}(-\mathbf{k}\lambda) = \epsilon_\mu(-\mathbf{k}\lambda) . \quad (\text{A.3c})$$

In contrast to Subjects. 2.2.1 and 2.2.2 the projections of total deuteron and trinucleon angular momenta M_I and \mathcal{M}_B as well as the projection of the nucleon spin m_s are notationally indicated in the hadronic states. All spin projections in those states refer to the direction of the incoming photon momentum \mathbf{k}_γ^{dis} in disintegration as quantization axis.

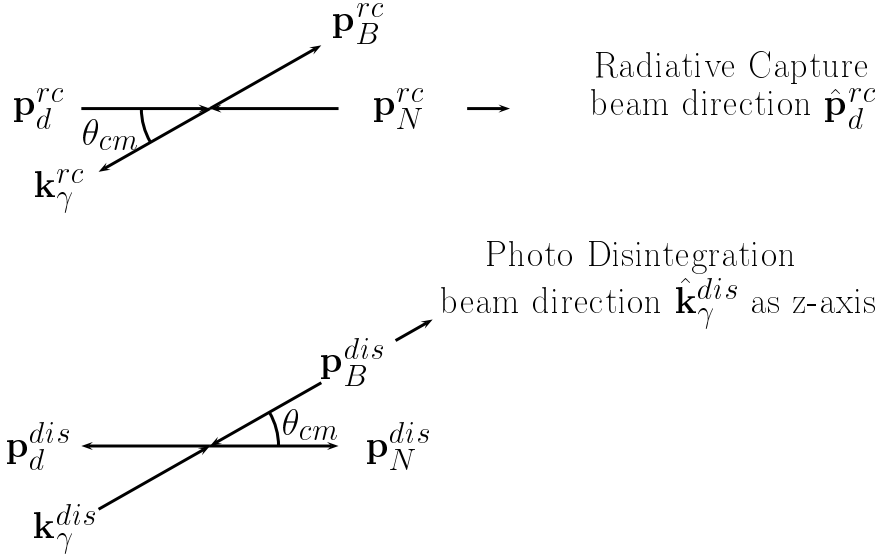


Figure A.1. Kinematic situations of nucleon-deuteron radiative capture and of two-body photo disintegration of the trinucleon bound state in the c.m. system. The relation between momenta connected by time reversal and the respective beam axes are shown.

The only spin observables studied in this paper are analyzing powers in radiative capture. In contrast to the quantization axis used for the matrix elements (A.2), the polarization of the deuteron and the nucleon are defined with respect to their respective momentum direction. Thus, either the spin dependence of the matrix element $\langle s_f | M^{rc} | s_i \rangle$ has to be turned to the new quantization axis or the deuteron and nucleon spin operators $\{S_i, S_{jk}\}$ and σ_i have to be transformed to them by the rotation $D(\alpha\beta\gamma) = \exp(-i\alpha J_z/\hbar)\exp(-i\beta J_y/\hbar) \times \exp(-i\gamma J_z/\hbar)$, \mathbf{J} being the general angular momentum operator creating the rotation, i.e.,

$$S^i \longrightarrow D(0\theta_{cm}0)S^i D^\dagger(0\theta_{cm}0) \quad , \quad (\text{A.4a})$$

$$\sigma_i \longrightarrow D(0 - (\pi - \theta_{cm})0)\sigma_i D^\dagger(0 - (\pi - \theta_{cm})0) \quad . \quad (\text{A.4b})$$

The transformation of S_{jk} follows from Eq. (A.4a). With those transformations the spin observables (2.18) of Subsect. 2.2.3 are calculated. When the dependence of observables on the photon helicity and on the trinucleon spin are studied, no additional transformations of states or operators will be required.

Appendix B. Details of Calculation

This appendix calculates the current matrix element of two-body photo disintegration of the trinucleon bound state $\langle \psi_{\alpha}^{-}(\mathbf{q}_f) \nu_{\alpha_f}(Nd) | j^{\mu}(\mathbf{k}_{\gamma}, \mathbf{p}_N + \mathbf{p}_d + \mathbf{p}_B) \epsilon_{\mu}(\mathbf{k}_{\gamma}, \lambda) | B \rangle$. The calculation is done in the c.m. system, i.e., $\mathbf{p}_d = -\mathbf{p}_N$, $\mathbf{p}_B = -\mathbf{k}_{\gamma}$. The calculation uses a nonrelativistic potential model for the hadronic interaction. The baryon energies are employed in nonrelativistic forms.

B.1 Basis States

The basis states $|pq\nu\rangle_{\alpha}$ describing the internal motion of three baryons are defined in Eq. (2.2) of ref. [1]. The discrete quantum numbers of the basis states, abbreviated by ν are indicated in Fig. B.1. The subscript α at the states defines the role of particles as pair and spectator; this is why the subscript α at quantum numbers is omitted, unless ambiguities could arise. In Fig. B.1 the (Ij) coupling scheme is used, i.e.,

$$\nu(Ij) = \{[L(s_{\beta}s_{\gamma})S]I(ls)j\} \mathcal{J}M_J \{(t_{\beta}t_{\gamma})Tt\} \mathcal{T}M_T Bb. \quad (\text{B.1})$$

The orbital angular momentum of the pair L and of the spectator l are first

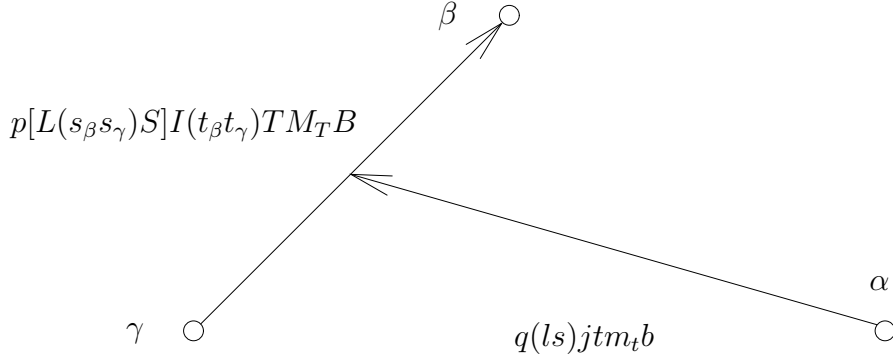


Figure B.1. Three-baryon Jacobi momenta, and discrete quantum numbers. The spectator baryon is labeled α , the pair is made up of baryons β and γ .

coupled with their respective spins S and s to total pair and spectator angular momenta I and j , which are then combined to total angular momentum \mathcal{J} with projection \mathcal{M}_J ; the parity quantum number can be derived according to $\Pi = (-)^L (-)^l$. The isospin coupling of the pair isospin T and of the spectator isospin t is done correspondingly for total isospin \mathcal{T} with projection \mathcal{M}_T . In the trinucleon bound states and in nucleon-deuteron scattering without Coulomb interaction only basis states with total isospin $\mathcal{T} = \frac{1}{2}$ are needed. The additional quantum numbers (Bb) give the baryon characteristics of the pair and of the spectator, $B = 1(0)$ standing for a two-nucleon (nucleon- Δ) pair, $b = \frac{1}{2}(-\frac{1}{2})$

for a spectator nucleon (Δ); baryon characteristics could be read off from the individual spin and isospin quantum numbers s and t ; the additional quantum numbers (Bb) are introduced for convenience. The discrete quantum numbers, distinct from the continuous Jacobi momenta p and q , are abbreviated by $\nu(Ij)$.

Practical calculations suggest other coupling schemes for different parts of the numerics. The ($\mathcal{L}S$) coupling scheme

$$\nu(\mathcal{L}S) = \{(Ll)\mathcal{L}[(s_\beta s_\gamma)Ss]S\}\mathcal{J}M_J\{(t_\beta t_\gamma)Tt\}\mathcal{T}M_T Bb \quad (\text{B.2})$$

and the channel-spin coupling scheme

$$\nu(lK) = \{l([L(s_\beta s_\gamma)S]Is)K\}\mathcal{J}M_J\{(t_\beta t_\gamma)Tt\}\mathcal{T}M_T Bb \quad (\text{B.3})$$

are also used. The transformation between coupling schemes

$$\langle \nu(\mathcal{L}S) | \nu(Ij) \rangle = \hat{\mathcal{L}}\hat{S}\hat{I}\hat{j} \begin{Bmatrix} L & l & \mathcal{L} \\ S & s & S \\ I & j & \mathcal{J} \end{Bmatrix}, \quad (\text{B.4a})$$

$$\langle \nu(lK) | \nu(Ij) \rangle = (-)^{l+K+I+j} \hat{K}\hat{j} \begin{Bmatrix} I & s & K \\ l & \mathcal{J} & j \end{Bmatrix}, \quad (\text{B.4b})$$

$$\begin{aligned} \langle \nu(lK)(\mathcal{L}S) | \nu(\mathcal{L}S) \rangle &= (-)^{L+S+s+K+S+J-L} \hat{\mathcal{L}}\hat{S}\hat{I}\hat{K} \\ &\times \begin{Bmatrix} S & L & I \\ K & s & S \end{Bmatrix} \begin{Bmatrix} L & S & K \\ \mathcal{J} & l & \mathcal{L} \end{Bmatrix}, \end{aligned} \quad (\text{B.4c})$$

using the abbreviation $\hat{a} = \sqrt{2a+1}$, are unitary. They do not involve isospin and baryon content and are independent from the continuous Jacobi momenta (pq) at which the transformations are carried out.

We calculate the matrix element $\langle \psi_\alpha^-(\mathbf{q}_f)\nu_{\alpha_f}(Nd) | j^\mu(\mathbf{k}_\gamma, \mathbf{p}_B)\epsilon_\mu(\mathbf{k}_\gamma\lambda) | B \rangle$ of photo disintegration first and then use time reversal for obtaining the corresponding one of radiative capture. The latter step is described in Appendix A. The matrix element has three ingredients, i.e., the current operator $j^\mu(\mathbf{k}_\gamma, \mathbf{p}_B)\epsilon_\mu(\mathbf{k}_\gamma\lambda)$, the initial bound state $|B\rangle$ and the final scattering state $\langle \psi_\alpha^-(\mathbf{q}_f)\nu_{\alpha_f}(Nd) |$. Since the three baryons can be considered identical, whereas the employed basis $|pq\nu\rangle_\alpha$ is not totally antisymmetric, explicit antisymmetrization has to be carried out with the permutation operator $P = P_{123} + P_{321}$. The permutation operator P is described in ref. [2].

B.2 Three-Nucleon Bound State $|B\rangle$

The three-nucleon bound state $|B\rangle$ is obtained from the corresponding Faddeev amplitude $|\psi_\alpha\rangle$ according to

$$|B\rangle = N(1 + P)|\psi_\alpha\rangle \quad (\text{B.5a})$$

N being the normalization factor ensuring $\langle B|B\rangle = 1$. The Faddeev amplitude $|\psi_\alpha\rangle$ is best calculated in (Ij) coupling, whereas for the computation of the current matrix element (\mathcal{LS}) coupling is the better choice, i.e.,

$$\begin{aligned} \langle pq\nu(\mathcal{LS})|B\rangle = & N \int dp' dq' p'^2 q'^2 \sum_{\nu'(\mathcal{L}'\mathcal{S}')} \sum_{I'j'} \langle pq\nu(\mathcal{LS})|(1+P)|p'q'\nu'(\mathcal{L}'\mathcal{S}')\rangle \\ & \times \langle \nu'(\mathcal{L}'\mathcal{S}')|\nu'(I'j')\rangle \langle p'q'\nu'(I'j')|\psi_\alpha\rangle. \end{aligned} \quad (\text{B.5b})$$

B.3 The Three-Nucleon Scattering State $|\psi_\alpha^{(+)}(\mathbf{q})\nu_\alpha(Nd)\rangle$

The antisymmetrized nucleon-deuteron scattering state of internal motion $|\psi_\alpha^{(+)}(\mathbf{q})\nu_\alpha(Nd)\rangle$ is obtained from the corresponding plane-wave state $|\phi_\alpha(\mathbf{q})\nu_\alpha(Nd)\rangle$ by the full resolvent $G(Z)$, i.e.,

$$|\psi_\alpha^{(+)}(\mathbf{q})\nu_\alpha(Nd)\rangle = i0G(E_\alpha(\mathbf{q}) + i0)(1+P)/\sqrt{3}|\phi_\alpha(\mathbf{q})\nu_\alpha(Nd)\rangle, \quad (\text{B.6a})$$

$$\begin{aligned} |\psi_\alpha^{(+)}(\mathbf{q})\nu_\alpha(Nd)\rangle = & (1+P)/\sqrt{3} \left[1 + G_0(E+i0)T_\alpha(E+i0)G_0(E+i0)U(E+i0) \right] \\ & \times |\phi_\alpha(\mathbf{q})\nu_\alpha(Nd)\rangle|_{E=E_\alpha(\mathbf{q})}. \end{aligned} \quad (\text{B.6b})$$

In Eq. (B.6b) the two-baryon transition matrix $T_\alpha(Z)$ and three-particle multi-channel transition matrix $U(Z)$ are introduced; they are defined in ref. [1]. In this section, as in ref. [1], the three-particle c.m. part of the kinetic energy operator is left out; $E_\alpha(\mathbf{q})$ is the internal nucleon-deuteron energy corresponding to the relative momentum \mathbf{q} , i.e., $E_\alpha(\mathbf{q}) = E_{Nd}(\mathbf{q}\mathbf{K}) - \mathbf{K}^2/(6m_N)$ according to Eq. (2.6b). The two-baryon interaction is separably expanded. Thus, the plane-wave state has the following form

$$\begin{aligned} |\phi_\alpha(\mathbf{q})\nu_\alpha(Nd)\rangle & = G_0(E_\alpha(\mathbf{q}) + i0) |g_\alpha^{(i_0\pi_0 I_0 T_0)} M_I M_{T_0}\rangle | \mathbf{q} s_0 m_s t_0 m_{t_0} b_0 \rangle_\alpha, \end{aligned} \quad (\text{B.7a})$$

$$\begin{aligned} |\phi_\alpha(\mathbf{q})\nu_\alpha(Nd)\rangle & = G_0(E_\alpha(\mathbf{q}) + i0) \sum_{\Pi\mathcal{J}\mathcal{M}_\mathcal{J}\mathcal{T}\mathcal{M}_\mathcal{T}} \sum_{jm_j lm_l} |i_0 q \chi(I_0 j) \Pi \mathcal{J} \mathcal{M}_\mathcal{J} \mathcal{T} \mathcal{M}_\mathcal{T}\rangle_\alpha \\ & \times \langle I_0 M_I j m_j | \mathcal{J} \mathcal{M}_\mathcal{J} \rangle \langle T_0 M_{T_0} t_0 m_{t_0} | \mathcal{T} \mathcal{M}_\mathcal{T} \rangle \langle l m_l s_0 m_s | j m_j \rangle Y_{lm_l}^*(\hat{\mathbf{q}}) \end{aligned} \quad (\text{B.7b})$$

with the quantum numbers $\pi_0 = +, I_0 = 1, T_0 = M_{T_0} = 0$ and $s_0 = t_0 = b_0 = \frac{1}{2}$. The choice of the spin projections M_I and m_s specifies experimental conditions, and the choice of the isospin projection $m_{t_0} = +\frac{1}{2}$ makes the calculation refer to proton-deuteron scattering. Eq.(B.7a) relates the deuteron state back to the corresponding form factor $|g_\alpha^{(i_0\pi_0 I_0 T_0)} M_I M_{T_0}\rangle$ of the separable expansion; in Eq. (B.7b) the partial-wave coupled states $|i_0 q \chi(I_0 j) \Pi \mathcal{J} \mathcal{M}_\mathcal{J} \mathcal{T} \mathcal{M}_\mathcal{T}\rangle_\alpha$, introduced in Eq.(2.4) of Ref.[2] for the description of nucleon-deuteron scattering,

are used. The practical computation of the scattering state

$$\begin{aligned}
|\psi_\alpha^{(+)}(\mathbf{q})\nu_\alpha(Nd)\rangle &= (1+P)/\sqrt{3}G_0(E+i0) \\
&\times \left[1 + |\mathbf{g}_\alpha\rangle\mathcal{T}_\alpha(E+i0)\langle\mathbf{g}_\alpha|G_0(E+i0)U(E+i0)G_0(E+i0)\right] \Big|_{E=E_\alpha(\mathbf{q})} \\
&\times \sum_{\Pi\mathcal{J}\mathcal{M}_\mathcal{J}\mathcal{T}\mathcal{M}_\mathcal{T}} \sum_{jm_jlm_l} |i_0q\chi(I_0j)\Pi\mathcal{J}\mathcal{M}_\mathcal{J}\mathcal{T}\mathcal{M}_\mathcal{T}\rangle_\alpha \\
&\times \langle I_0M_Ijm_j|\mathcal{J}\mathcal{M}_\mathcal{J}\rangle\langle T_0M_{T_0}t_0m_{t_0}|\mathcal{T}\mathcal{M}_\mathcal{T}\rangle\langle lm_l s_0 m_s|jm_j\rangle Y_{lm_l}^*(\hat{\mathbf{q}}) \quad (\text{B.8a})
\end{aligned}$$

$$\begin{aligned}
|\psi_\alpha^{(+)}(\mathbf{q})\nu_\alpha(Nd)\rangle &= (1+P)/\sqrt{3}G_0(E+i0) \sum_{\Pi\mathcal{J}\mathcal{M}_\mathcal{J}\mathcal{T}\mathcal{M}_\mathcal{T}} \sum_{jm_jlm_l} \\
&\times \left[|i_0q\chi(I_0j)\Pi\mathcal{J}\mathcal{M}_\mathcal{J}\mathcal{T}\mathcal{M}_\mathcal{T}\rangle_\alpha + \right. \\
&\sum_{\chi_c} \sum_{i'_c} \int_0^\infty q_c^2 dq_c |i'_c q_c \chi_c(I_c j_c)\Pi\mathcal{J}\mathcal{M}_\mathcal{J}\mathcal{T}\mathcal{M}_\mathcal{T}\rangle (i'_c|\mathcal{T}(E+i0, q_c \chi_c(I_c j_c))|i_c) \\
&\quad \left. \times (i_c q_c \chi_c(I_c j_c)|X^{\Pi\mathcal{J}\mathcal{T}}(E+i0)|iq\chi(Ij)) \right] \Big|_{E=E_\alpha(\mathbf{q})} \\
&\times \langle I_0M_Ijm_j|\mathcal{J}\mathcal{M}_\mathcal{J}\rangle\langle T_0M_{T_0}t_0m_{t_0}|\mathcal{T}\mathcal{M}_\mathcal{T}\rangle\langle lm_l s_0 m_s|jm_j\rangle Y_{lm_l}^*(\hat{\mathbf{q}}) \quad (\text{B.8b})
\end{aligned}$$

proceeds according to the strategy suggested by the separable expansion:

- The operator $G_0(E+i0)U(E+i0)G_0(E+i0)$ is computed between states $|iq\chi(Ij)\Pi\mathcal{J}\mathcal{M}_\mathcal{J}\mathcal{T}\mathcal{M}_\mathcal{T}\rangle_\alpha$ in (Ij) coupling; it and $\mathcal{T}_\alpha(Z)$ are diagonal in the three-particle quantum numbers $(\Pi\mathcal{J}\mathcal{M}_\mathcal{J}\mathcal{T}\mathcal{M}_\mathcal{T})$ and independent of $\mathcal{M}_\mathcal{J}$ and $\mathcal{M}_\mathcal{T}$; for $G_0(E+i0)U(E+i0)G_0(E+i0)$ half-off-shell elements are required. Eq. (B.8b) uses the matrix elements $(i_c q_c \chi_c(I_c j_c)|X^{\Pi\mathcal{J}\mathcal{T}}(E+i0)|iq\chi(Ij))$ and $(i'_c|\mathcal{T}(E+i0, q_c \chi_c(I_c j_c))|i_c)$ of $G_0(E+i0)U(E+i0)G_0(E+i0)$ and of $\mathcal{T}_\alpha(E+i0)$ as introduced in ref. [2].
- The number of form factors $|\mathbf{g}_\alpha\rangle$, i.e., the assumption on the dynamics, truncates the number of arising partial waves $|iq\chi(Ij)\Pi\mathcal{J}\mathcal{M}_\mathcal{J}\mathcal{T}\mathcal{M}_\mathcal{T}\rangle_\alpha$ for each total angular momentum \mathcal{J} . The truncation in \mathcal{J} comes from the structure of the current, the matrix element of which is computed.
- $(\mathcal{L}S)$ coupled components ${}_\alpha\langle pq\nu(\mathcal{L}S)|\psi_\alpha^{(+)}(\mathbf{q})\nu_\alpha(Nd)\rangle$ of the scattering state are determined; those components are most convenient for the full calculation of the current matrix element. The permutation operator P is applied in (Ij) coupling and the result is then transformed to $(\mathcal{L}S)$ coupling.

The three-nucleon scattering state $|\psi_\alpha^{(+)}(\mathbf{q})\nu_\alpha(Nd)\rangle$ can be computed according to the steps explained in this subsection and the current matrix element

$\langle \psi_{\alpha}^{(-)}(\mathbf{q}_f) \nu_{\alpha_f}(Nd) | j^{\mu}(\mathbf{k}_{\gamma}, \mathbf{p}_N + \mathbf{p}_d + \mathbf{p}_B) \epsilon_{\mu}(\mathbf{k}_{\gamma} \lambda) | B \rangle$ can be obtained from it and the bound state $|B\rangle$. We use that calculational avenue for numerical checks, but prefer a more direct alternative strategy for determining the current matrix element:

$$\begin{aligned} & \langle \psi_{\alpha}^{(-)}(\mathbf{q}_f) \nu_{\alpha_f}(Nd) | j^{\mu}(\mathbf{k}_{\gamma}, \mathbf{p}_N + \mathbf{p}_d + \mathbf{p}_B) \epsilon_{\mu}(\mathbf{k}_{\gamma} \lambda) | B \rangle \\ &= \langle \phi_{\alpha}(\mathbf{q}_f) \nu_{\alpha_f} | \Omega(E + i0)(1 + P) / \sqrt{3} j^{\mu}(\mathbf{k}_{\gamma}, \mathbf{p}_N + \mathbf{p}_d + \mathbf{p}_B) \epsilon_{\mu}(\mathbf{k}_{\gamma} \lambda) | B \rangle \Big|_{E=E_{\alpha_f}(\mathbf{q}_f)} \end{aligned} \quad (\text{B.9a})$$

$$\Omega(Z) = 1 + U(Z)G_0(Z)T_{\alpha}(Z)G_0(Z), \quad (\text{B.9b})$$

$$\Omega(Z) = \sum_{n=0}^{\infty} (PT_{\alpha}(Z)G_0(Z))^n. \quad (\text{B.9c})$$

Eqs. (B.9) are consistent with Eq. (B.6b) which relates the scattering state $|\psi_{\alpha}^{(+)}(\mathbf{q}_i) \nu_{\alpha_i}(Nd)\rangle$ to the multi-channel transition matrix $U(E_{\alpha}(\mathbf{q}) + i0)$. Since $U(Z)$ satisfies an integral equation [1], that property carries over to the current matrix element (B.9a), i.e.,

$$\begin{aligned} & \Omega(E + i0)(1 + P) / \sqrt{3} j^{\mu}(\mathbf{k}_{\gamma}, \mathbf{p}_N + \mathbf{p}_d + \mathbf{p}_B) \epsilon_{\mu}(\mathbf{k}_{\gamma} \lambda) | B \rangle \\ &= (1 + P) / \sqrt{3} j^{\mu}(\mathbf{k}_{\gamma}, \mathbf{p}_N + \mathbf{p}_d + \mathbf{p}_B) \epsilon_{\mu}(\mathbf{k}_{\gamma} \lambda) | B \rangle \\ &+ PT_{\alpha}(E + i0)G_0(E + i0) \left[\Omega(E + i0)(1 + P) / \sqrt{3} j^{\mu}(\mathbf{k}_{\gamma}, \mathbf{p}_N + \mathbf{p}_d + \mathbf{p}_B) \epsilon_{\mu}(\mathbf{k}_{\gamma} \lambda) | B \rangle \right] \end{aligned} \quad (\text{B.10})$$

with $E = E_{\alpha_f}(\mathbf{q}_f)$. The integral equation (B.10) has the same kernel $PT_{\alpha}(E + i0)G_0(E + i0)$ as the corresponding one for $U(E + i0)$ and can therefore be solved with the same numerical techniques, just its driving term $(1 + P) / \sqrt{3} j^{\mu}(\mathbf{k}_{\gamma}, \mathbf{p}_N + \mathbf{p}_d + \mathbf{p}_B) \epsilon_{\mu}(\mathbf{k}_{\gamma} \lambda) | B \rangle$ is different. When taking the scalar product of the correlated state resulting from the integral equation (B.10) with the channel state $\langle \phi_{\alpha}(\mathbf{q}_f) \nu_{\alpha_f}(Nd) |$, the required current matrix element follows. This alternative calculational scheme, based on (B.10), is the one usually employed for the numerics of the paper; it solves the integral equation for the scattering state $|\psi_{\alpha}^{(+)}(\mathbf{q}) \nu_{\alpha}(Nd)\rangle$ implicitly when forming the current matrix element.

B.4 Current Operator

We calculate the current matrix element of two-body disintegration of the trinucleon bound states for the current operator $j^{\mu}(\mathbf{k}_{\gamma}, \mathbf{p}_N + \mathbf{p}_d + \mathbf{p}_B) \epsilon_{\mu}(\mathbf{k}_{\gamma} \lambda)$ in the c.m. system, i.e., $\mathbf{p}_N = -\mathbf{p}_d$, $\mathbf{p}_B = -\mathbf{k}_{\gamma}$, assuming that the momentum of the real photon defines the z direction, i.e., $\hat{\mathbf{k}}_{\gamma} = \hat{\mathbf{e}}_3$ and $\lambda = \pm 1$. The current

operator has the decomposition

$$\begin{aligned} & j^\mu(k_\gamma \hat{\mathbf{e}}_3, -k_\gamma \hat{\mathbf{e}}_3) \epsilon_\mu(k_\gamma \hat{\mathbf{e}}_3 \lambda) \\ &= -\frac{1}{\sqrt{2}} \sum_j \sqrt{4\pi} i^j \sqrt{2j+1} \left[T_{elec\lambda}^{(j)}(k_\gamma/\hbar) + \lambda T_{magn\lambda}^{(j)}(k_\gamma/\hbar) \right] \end{aligned} \quad (\text{B.11})$$

into electric and magnetic multipoles, i.e., $T_{elec\ m_j}^{(j)}(k)$ and $T_{magn\ m_j}^{(j)}(k)$ with $k = k_\gamma/\hbar$ and $k_\gamma = |\mathbf{k}_\gamma|$ for the rest of this appendix. In the c.m. system the formal parametric dependence on the total momentum $\mathbf{K}' + \mathbf{K} = -\mathbf{k}_\gamma$ is dropped. The multipoles are defined by

$$T_{elec\ m_j}^{(j)}(k) = -\left[\sqrt{\frac{j+1}{2j+1}} T_{m_j}^{([j-1,1]j)}(k) + \sqrt{\frac{j}{2j+1}} T_{m_j}^{([j+1,1]j)}(k) \right], \quad (\text{B.12a})$$

$$T_{magn\ m_j}^{(j)}(k) = T_{m_j}^{([j,1]j)}(k) \quad (\text{B.12b})$$

with

$$T_{m_j}^{([I,1]j)}(k) = \frac{(-i)^j}{4\pi} \int d^2\hat{\mathbf{k}} \left[Y^{(I)}(\hat{\mathbf{k}}) \otimes j^{(1)}(\hbar\mathbf{k}) \right]_{m_j}^{(j)}. \quad (\text{B.12c})$$

In Eq.(B.12c) $Y^{(I)}(\hat{\mathbf{k}})$ is the spherical tensor corresponding to the spherical harmonics $Y_{Im_I}(\hat{\mathbf{k}})$, $j^{(1)}(\hbar\mathbf{k})$ the spherical tensor corresponding to the spatial part of the corresponding current $j^\mu(\hbar\mathbf{k}, \mathbf{K}' + \mathbf{K})$. The electric multipole operator is employed in the Siegert form

$$T_{elec\ m_j}^{(j)}(k) = -\sqrt{\frac{2j+1}{j}} T_{m_j}^{([j+1,1]j)}(k) - \sqrt{\frac{j+1}{j}} \frac{1}{\hbar k} \left[H, T_{coul\ m_j}^{(j)}(k) \right] \quad (\text{B.13a})$$

with the Coulomb multipole

$$T_{coul\ m_j}^{(j)}(k) = T_{m_j}^{([j,0]j)}(k) = \frac{(-i)^j}{4\pi} \int d^2\hat{\mathbf{k}} Y_{jm_j}(\hat{\mathbf{k}}) \rho(\hbar\mathbf{k}), \quad (\text{B.13b})$$

$\rho(\hbar k)$ being the Fourier transform of the charge-density operator with normalization $\rho(0) = 1$. The form (B.13a) follows from current conservation; the hadronic Hamiltonian H includes the c.m. motion of the baryons. As is well known, the Siegert form of the electric multipole operator takes exchange two-baryon currents into account, even if the Coulomb multipole is derived from a charge density, composed of one-baryon operators only as done in the calculation of this paper.

For many low-energy photo processes the electric dipole makes the dominant

contribution to the current.

$$\begin{aligned} & \langle \psi_{\alpha}^{(-)}(\mathbf{q}_f) \nu_{\alpha_f}(Nd) | T_{elec\ m_j}^{(1)}(k_{\gamma}/\hbar) | B \rangle \\ &= \langle \psi_{\alpha}^{-}(\mathbf{q}_f) \nu_{\alpha_f}(Nd) | (-)\sqrt{3}T_{m_j}^{[2,1]}(k_{\gamma}/\hbar) - \sqrt{2}cT_{coul\ m_j}^{(1)}(k_{\gamma}/\hbar) | B \rangle \end{aligned} \quad (\text{B.14a})$$

$$\begin{aligned} &= \langle \psi_{\alpha}^{(-)}(\mathbf{q}_f) \nu_{\alpha_f}(Nd) | (-)\sqrt{3}T_{m_j}^{[2,1]}(k_{\gamma}/\hbar) \\ &\quad - \sqrt{2}c \int d^3x j_1(k_{\gamma}x/\hbar) Y_{1m_j}(\hat{\mathbf{x}}) \rho(\mathbf{x}) | B \rangle. \end{aligned} \quad (\text{B.14b})$$

That electric dipole operator is still exact. However, in applications it is often used in configuration space as in Eq.(B.14b) and in the long-wavelength limit, $k_{\gamma}x/\hbar \ll 1$, in which the first term $T_{m_j}^{[2,1]}(k_{\gamma}/\hbar)$ can be neglect and the regular spherical Bessel function of order 1, $j_1(k_{\gamma}x/\hbar)$ is approximated by $k_{\gamma}x/3\hbar$. Taking the charge operator $\rho(\mathbf{x})$ as single-baryon operator

$$\rho(\mathbf{x}) = \sum_i \frac{e_p}{2} (1 + \tau_3(i)) \delta(\mathbf{x} - \mathbf{x}_i), \quad (\text{B.15a})$$

the sum on i extending over all baryons, $\tau_3(i)$ being the isospin projection with values $\pm 1/2$ for nucleons and with values $\pm 3/2, \pm 1/2$ for a Δ -isobar, e_p being the positive elementary charge, the long-wavelength electric dipole operator takes the form

$$\begin{aligned} & \langle \psi_{\alpha}^{-}(\mathbf{q}_f) \nu_{\alpha_f}(Nd) | T_{elec\ m_1}^{(1,l.w.)}(k_{\gamma}/\hbar) | B \rangle \\ & \approx \frac{(-)k_{\gamma}c}{\sqrt{4\pi}\hbar} \langle \psi_{\alpha}^{-}(\mathbf{q}_f) \nu_{\alpha_f}(Nd) | \sum_i \frac{e_p}{2} (1 + \tau_3(i)) (x_i)_{m_1}^{(1)} | B \rangle. \end{aligned} \quad (\text{B.15b})$$

Our calculation is in momentum space. Thus, the use of the configuration space operator (B.15b) is unnecessary. Nevertheless, we are able to simulate the use of the approximate operator (B.15b) by a trick:

- Calculate the matrix element (B.15b) for a fictions unrealistically small photon momentum \mathcal{K}_{γ} for which the approximation $j_1(\mathcal{K}_{\gamma}x/\hbar) \approx \mathcal{K}_{\gamma}x/3\hbar$ with high precision.
- Since the dependence on the physical photon momentum k_{γ} is linear in Eq.(B.15b) the proper matrix element for the operator (B.15b) is obtained by scaling with the factor $k_{\gamma}/\mathcal{K}_{\gamma}$, i.e.,

$$\begin{aligned} & \langle \psi_{\alpha}^{-}(\mathbf{q}_f) \nu_{\alpha_f}(Nd) | T_{elec\ m_1}^{(1,l.w.)}(k_{\gamma}/\hbar) | B \rangle \\ &= \frac{k_{\gamma}}{\mathcal{K}_{\gamma}} \langle \psi_{\alpha}^{-}(\mathbf{q}_f) \nu_{\alpha_f}(Nd) | T_{elec\ m_1}^{(1)}(\mathcal{K}_{\gamma}/\hbar) | B \rangle. \end{aligned} \quad (\text{B.15c})$$

B.5 Instability Problem in Calculation of Current Matrix Elements

The physics results of this paper depend on matrix elements of the e.m. current $J^{\mu}(\mathbf{Q})$ according to Eqs. (2.4), (2.11b) and (2.14a). The computation of

those current matrix elements is quite involved and will not be spelt out in detail in this appendix. The computation is based on the multipole decomposition of the current and on partial-wave decompositions of the initial and final baryonic states. The computation encounters particular numerical problems: The contributions arising from higher current multipoles and from higher angular momenta in the hadronic states get computationally split up into series of rather large numbers with alternating signs, the full results being comparatively small; the straight-forward evaluation of those series becomes instable. We are unable to cope with that instability properly and to avoid it for good. Nevertheless, we believe that the results, presented in this paper, are computationally quite reliable. This appendix tries to give convincing reasons for our claim.

The current has one- and two-body contributions. For computational purposes, each current contribution is tensorially recoupled as tensor product of orbital, spin and isospin operators. The matrix elements of $T_{m_j}^{([I,a]j)}(k)$ with $k = k_\gamma/\hbar$ take the general form

$$\begin{aligned} & \langle \mathbf{p}' \mathbf{q}' | T_{m_j}^{([I,a]j)}(k) | \mathbf{p} \mathbf{q} \rangle \\ &= (-i)^j (4\pi)^{\frac{1}{2}} \sum_{\kappa} RK(a, b, e, j, I; \kappa) \int d^2 \hat{\mathbf{k}} f_p(k, p_-, p_+, v_p) f_q(k, q_-, q_+, v_q) \\ & \quad \times \left(Y^{(\kappa)}(\hat{\mathbf{k}}) \otimes \left[\mathcal{O}^{(c)}(c_{p_+}, c_{p_-}, c_p, c_q) \otimes S^{(d)} \right]^{(e)} \right)_{m_j}^{(j)}, \end{aligned} \quad (\text{B.16})$$

$\mathcal{O}^{(c)}$ being the orbital and $S^{(d)}$ being the spin part. The matrix elements of $T_{m_j}^{([I,a]j)}(k)$ are computed in partial-wave basis with the operators acting on the three-baryon bound state $|B\rangle$, i.e.,

$$\begin{aligned} & \langle \mathcal{J}' M_{J'} | T_{m_j}^{([I,a]j)}(k) | B \rangle \\ &= (-)^{\mathcal{J}' - M_{J'}} \begin{pmatrix} \mathcal{J}' & j & \frac{1}{2} \\ -M_{J'} & m_j & \mathcal{M}_B \end{pmatrix} \langle \mathcal{J}' || T^{([I,a]j)}(k) || B \rangle, \end{aligned} \quad (\text{B.17})$$

$1/2$ being the total angular momentum of the bound state and \mathcal{M}_B its projection. For a two-body contribution the formal structure of the resulting matrix

elements is as follows:

$$\begin{aligned}
& \langle p'q'[(L'l)\mathcal{L}'(S's')\mathcal{S}']\mathcal{J}'|T^{([Ia]j)}(k)|B\rangle \\
&= (-i)^j (4\pi)^{\frac{3}{2}} \sum_{\nu=\{Ll\mathcal{L}Ss\mathcal{S}\}} \langle (S's')\mathcal{S}'||S^{(d)}||(\mathcal{S}s)\mathcal{S}\rangle \\
&\quad \times \sum_{\kappa} RK(a, b, e, j, I; \kappa) \sum_{\sigma} RS(c, d, e, j; \mathcal{L}', \mathcal{S}', \mathcal{J}', \mathcal{L}, \mathcal{S}, \frac{1}{2}; \kappa, \sigma) \\
&\quad \times \sum_{\gamma_p \varphi_p \gamma_q \varphi_q} (-)^{c+\sigma} \hat{\gamma}_p \hat{\varphi}_p \hat{\gamma}_q \hat{\varphi}_q \hat{c} \hat{\kappa} \hat{\sigma} \hat{\mathcal{L}}' \hat{\mathcal{L}} \begin{pmatrix} \varphi_p & \varphi_q & \kappa \\ 0 & 0 & 0 \end{pmatrix} \\
&\quad \times \begin{Bmatrix} c_p & c_q & c \\ \varphi_p & \varphi_q & \kappa \\ \gamma_p & \gamma_q & \sigma \end{Bmatrix} \begin{Bmatrix} L' & L & \gamma_p \\ l' & l & \gamma_q \\ \mathcal{L}' & \mathcal{L} & \sigma \end{Bmatrix} \sum_{\rho} RK(c_p, c_{p-}, c_{p+}, \gamma_p, \varphi_p; \rho) \\
&\quad \times \int_0^{\infty} p^2 dp \langle p'L' || P^{(\gamma_p)}(c_{p+}, \rho, \varphi_p) || pL \rangle \\
&\quad \times \int_0^{\infty} q^2 dq \langle q'l' || Q^{(\gamma_q)}(c_q, \varphi_q, \varphi_q) || ql \rangle \langle pq\nu | B \rangle. \tag{B.18}
\end{aligned}$$

Both formulae (B.16) and (B.18) are admittedly intransparent ones. The quantities RK and RS are of geometric nature and just combinations of coefficients like $3j$ and $6j$ symbols arising from several recouplings. However, the detailed forms of (B.16) and (B.18) are irrelevant for the following numerical consideration.

In Eq. (B.16) the complete momentum dependence is buried in the two functions $f_p(k, p_-, p_+, v_p)$ and $f_q(k, q_-, q_+, v_q)$. The function $f_p(k, p_-, p_+, v_p)$ is regular in \mathbf{k} , the limit $k = 0$ can be carried out without any problem, making that function independent of $\hat{\mathbf{k}}$ and v_p . In contrast, the function $f_q(k, q_-, q_+, v_q)$ carries a δ -function in \mathbf{k} , which gets integrated out by acting the operator of Eq. (B.16) on the three-baryon bound state, i.e., by forming $\langle \mathbf{p}'\mathbf{q}' | T_{m_j}^{([Ia]j)}(k) | B \rangle$; then the limit $k = 0$ can be performed leaving $Y^{(\kappa)}(\hat{\mathbf{k}})$ in (B.16) and in $\langle \mathbf{p}'\mathbf{q}' | T_{m_j}^{([Ia]j)}(k) | B \rangle$ the only dependence on $\hat{\mathbf{k}}$. As a consequence the tensor order

$$\kappa = 0, \quad \text{if } k = 0, \tag{B.19}$$

results. In Eq. (B.18) the characteristics of the considered current contribution enters by the non-negative integer parameters c_p, c_q and c with $c_q = 0$ or $c_q = 1$. One numerically dangerous part of the expression is the q -integration over the orbital operator $Q^{(\gamma_q)}(c_q, \varphi_q, \varphi_q)$ which weighs the bound-state wave function $\langle pq\nu | B \rangle$. Close inspection, e.g., according to Eq. (D.41) of ref. [23], shows that the chosen computation carries powers of the ratios q/k and q'/k which for momentum transfer k small compared with physically relevant q and q' in the

baryonic wave functions become unwantedly large. The numerical instability arises from the integration of those orbital operators $Q^{(\gamma_q)}(c_q, \varphi_q, \varphi_q)$ for which the contributing tensor order γ_q becomes large. That source for instability is p -dependent and therefore contributes to the p -integration; it enhances instabilities in the integration over $P^{(\gamma_p)}(c_{p+}, \rho, \varphi_p)$, which arise independently. We note, however, from the internal structure of the p -integral on $P^{(\gamma_p)}(c_{p+}, \rho, \varphi_p)$ that in the limit $k = 0$ the only contribution to $P^{(\gamma_p)}(c_{p+}, \rho, \varphi_p)$ is for vanishing φ_p , i.e.,

$$\varphi_p = 0, \quad \text{if } k = 0. \quad (\text{B.20})$$

The result follows from Eq. (D.14) of ref. [23]. Thus according to Eqs. (B.19) and (B.20) and according to the $9j$ -symbol in Eq. (B.18) $\varphi_q = 0$ as well as $\gamma_q = c_q$ in the limit $k = 0$. Of course, outside the limit $k = 0$ the tensor orders $\kappa > 0, \varphi_p > 0, \varphi_q > 0$ and $\gamma_q \neq c_q$ make contributions. Nevertheless, we observe a rapidly decreasing weight with increasing order γ_q , i.e., we observe numerical convergence and stability well before instable fluctuations set in with high tensor orders γ_q of $Q^{(\gamma_q)}(c_q, \varphi_q, \varphi_q)$.

In the table we give one example for the procedure and the reached numerical stability. The sample observable is the isovector magnetic form factor $F_M(Q)$ of the three-nucleon bound state, the contribution arising from the π -contact current is given. The observable in the table corresponds to the one plotted in the lower part of Fig. 7. The momentum transfer is called Q in that plot; it corresponds to the k in this appendix. The convergence with respect to the included maximal tensor order $\gamma_{q,max}$ of Eq. (B.18) is studied. Numerical instability sets in when the tensor order $\gamma_{q,onset}$ is computed.

Table: Contribution arising from the π -contact exchange current to the isovector trinucleon magnetic formfactor $F_M(Q)$

Q [fm $^{-1}$]	$\gamma_{q,max}$					$\gamma_{q,onset}$
	0	1	2	3	4	
0.001	-0.622761	-0.678250	-0.678250	-0.678250	-0.678250	6
0.01	-0.622743	-0.678231	-0.678231	-0.678231	-0.678231	8
0.1	-0.620939	-0.676272	-0.676289	-0.676289	-0.676289	> 8
1.0	-0.468388	-0.510500	-0.512039	-0.511955	-0.511955	> 9

Fig. B.2 gives another example for the onset of instability in the calculation of typical multipole matrix elements needed for the description of photo processes. In the examples of the figure very high multipoles are chosen, since for them the instability problem becomes most severe. Though the examples are for special multipoles, special quantum numbers and for a final scattering state without final-state interaction, the on-set of instability is observed in the same general regime of γ_q for all matrix elements and for the required realistic

case in which final-state interaction is included. For lower multipoles the onset of instability occurs at somewhat higher γ_q . A corresponding on-set of instability is seen, when calculating current matrix elements for inelastic electron scattering.

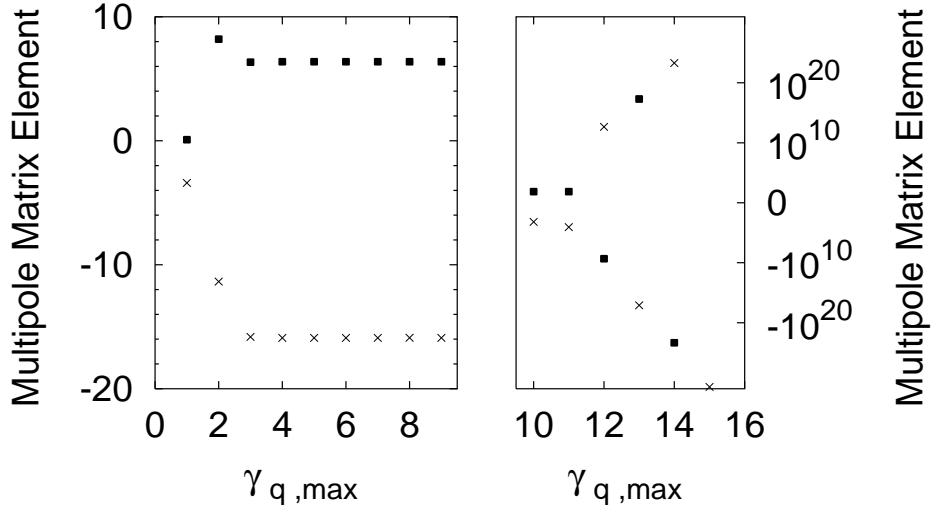


Figure B.2. Typical electric $E3$ (squares) and magnetic $M2$ (crosses) reduced multipole elements in units of $\text{fm}^{3/2}$, as function of $\gamma_{q,max}$. The multipoles are derived from the two-nucleon π -contact current as in the table, i.e., they are isovectors with respect to their isospin character and they refer to radiative capture at 19.8 MeV deuteron lab energy. In the examples the matrix elements are calculated in the Wigner-Eckart reduced form with respect to total angular momentum and isospin for symmetrized plane-wave impulse approximation in the channel-spin coupling of Eq. (B.3), keeping the first term of Eq. (B.8b) only, i.e., without final-state interaction: $\langle i_0 q \chi(l_f K_f) \Pi \mathcal{J} \mathcal{T} || G_0(E_f + i0)(1 + P) / \sqrt{3} T_{elec(magn)}^{(j)}(k_\gamma / \hbar) || B \rangle$; the three-particle quantum numbers $(\Pi \mathcal{J} \mathcal{T})$ are chosen to be $((-) 5/2 1/2)$, the spectator quantum numbers $(l_f K_f) = (3 1/2)$; for easier graphical presentation the multipole matrix elements are scaled by the numerical factor $1.5 * 10^6$.

References

1. Nemoto, S., Chmielewski, K., Haidenbauer, J., Oryu, S., Sauer, P. U., Schellingerhout, N. W.: *Few-Body Systems* **24**, 213 (1998).
2. Nemoto, S., Chmielewski, K., Haidenbauer, J., Meyer, U., Oryu, S., Sauer, P. U.: *Few-Body Systems* **24**, 241 (1998).
3. Nemoto, S., Chmielewski, K., Oryu, S., Sauer, P. U.: *Phys. Rev.* **C58**, 2599 (1998).
4. Chmielewski, K., Fonseca, A., Nemoto, S., Sauer, P. U.: *Few-Body Systems Suppl.* **10**, 335 (1998).
5. Glöckle, W., Witała, H., Hüber, D., Kamada, H., Golak, J.: *Phys. Rep.* **274**, 107 (1996).
6. Witała, H., Glöckle, W., Hüber, D., Golak, J., Kamada, H.: *Phys. Rev. Lett.* **81**, 1183 (1998).
7. Fonseca, A. C., Lehman, D. R.: *Phys. Rev.* **C48**, R503 (1993).
8. Fonseca, A. C., Lehman, D. R.: *Few-Body Systems* **28**, 189 (2000).
9. Anklin, H., de Bever, L. J., Buttazzoni, S., Glöckle, W., Golak, J., Honegger, A., Jourdan, J., Kamada, H., Kubon, G., Petijan, T., Qin, L. M., Sick, I., Steiner, P., Witała, H., Zeier, M., Zhao, J., Zihlmann, B.: *Nucl. Phys.* **A636**, 189 (1998).
10. Golak, J., Kamada, H., Witala, H., Gloeckle, W., Kuros, J., Skibinski, R., Kotlyar, V. V., Sagara, K., Akiyoshi, H.: *Phys. Rev.* **C62**, 54005 (2000).
11. Yuan, L. P., Chmielewski, K., Oelsner, M., Sauer, P. U., Fonseca, A. C., Adam Jr., J.: *Nucl. Phys.* **A689**, 433c (2001).
12. Strueve, W., Hajduk, C., Sauer, P. U., Theis, W.: *Nucl. Phys.* **A465**, 651 (1987).
13. Adam Jr., J., Truhlík, E., Adamova, D.: *Nucl. Phys.* **A492**, 556 (1989).
14. Adam Jr., J., Hajduk, C., Henning, H., Sauer, P. U., Truhlík, E.: *Nucl. Phys.* **A531**, 623 (1991).
15. Henning, H., Sauer, P. U., Theis, W.: *Nucl. Phys.* **A357**, 367 (1992).
16. Hajduk, C., Sauer, P. U., Strueve, W.: *Nucl. Phys.* **A405**, 581 (1983).
17. Lacombe, M., Loiseau, B., Richard, J. M., Vinh Mau, R., Côté, J., Pirès, P., de Turreil, R.: *Phys. Rev.* **C21**, 861 (1980).
18. Sauer, P. U.: *Nucl. Phys.* **A543**, 291c (1992).

19. Picklesimer, A., Rice, R. A., Brandenburg, R.: Phys. Rev. **C44**, 1359 (1991).
20. Baier, H., Bentz, W., Hajduk, C., Sauer, P. U.: Nucl. Phys. **A386**, 460 (1982).
21. Sauer, P. U., Henning, H.: Few-Body Systems **Suppl. 7**, 92 (1994).
22. Oelsner, M., Adam Jr., J., , Sauer, P. U., in: Proceedings of the 7th Conference Meson & Light Nuclei, Prague-Pruhonice 1998 (Adam Jr., J., ed.), World Scientific 1999, p.486.
23. Oelsner, M.: Ph.D. Thesis, University of Hannover 1999.
24. Amroun, A., *et al.*: Nucl. Phys. **A579**, 596 (1994).
25. Belt, B. D., *et al.*: Phys. Rev. Lett. **24**, 1120 (1970).
26. Vetterli, M. C., *et al.*: Phys. Rev.Lett. **54**, 1129 (1985).
27. Pitts, W. K., *et al.*: Phys. Rev. **C37**, 1 (1988).
28. Jourdan, J., *et al.*: Phys. Lett. **162B**, 269 (1985).
29. Schmid, G. J., *et al.*: Phys. Rev. **C53**, 35 (1996).
30. Browne, K. P., *et al.*: Phys. Rev. **C54**, 1538 (1996).
31. Kosiek, R., Müller, D, Pfeiffer, R.: Phys. Lett. **21**, 199 (1966).
32. Faul, D. D., *et al.*: Phys. Rev. Lett. **44**, 129 (1980).
33. Skopik, D. M., *et al.*: Phys. Rev. **C24**, 1791 (1981).